Resonant States in Negative Ions

Nicklas Brandefelt

AKADEMISK AVHANDLING

som med tillstånd av Stockholms universitet
framlägges till
offentlig granskning för avläggandet av
filosofie doktorsexamen
onsdagen den 12 september 2001, kl 10.00 i
rum FB52,
Stockholms centrum för fysik, astronomi och bioteknik,
Roslagstullsbacken 21, Stockholm

Department of Physics
Stockholm University
2001

Resonant States in Negative Ions
Nicklas Brandefelt
ISBN 91-7265-309-4 pp 1-60

(Atomfysik)
Stockholms universitet
Stockholms centrum för fysik, astronomi och bioteknik
Fysikum
S-106 91 Stockholm
SWEDEN

Universitetsservice US AB
STOCKHOLM 2001

Resonant States in Negative Ions

Nicklas Brandefelt

Abstract

Resonant states are multiply excited states in atoms and ions that have enough energy to decay by emitting an electron. The ability to emit an electron and the strong electron correlation (which is extra strong in negative ions) makes these states both interesting and challenging from a theoretical point of view. The main contribution in this thesis is a method, which combines the use of B splines and complex rotation, to solve the three-electron Schrödinger equation treating all three electrons equally. It is used to calculate doubly excited and triply excited states of ^4S symmetry with even parity in He^-. For the doubly excited states there are experimental and theoretical data to compare with. For the triply excited states there is only theoretical data available and only for one of the resonances. The agreement is in general good. For the triply excited state there is a significant and interesting difference in the width between our calculation and another method. A cause for this deviation is suggested. The method is also used to find a resonant state of ^4S symmetry with odd parity in H^{2-}. This state, in this extremely negative system, has been predicted by two earlier calculations but is highly controversial.

Several other studies presented here focus on two-electron systems. In one, the effect of the splitting of the degenerate $H(n = 2)$ thresholds in H^-, on the resonant states converging to this threshold, is studied. If a completely degenerate threshold is assumed an infinite series of states is expected to converge to the threshold. Here states of ^1P symmetry and odd parity are examined, and it is found that the relativistic and radiative splitting of the threshold causes the series to end after only three resonant states. Since the independent particle model completely fails for doubly excited states, several schemes of alternative quantum numbers have been suggested. We investigate the so called DESB (Doubly Excited Symmetry Basis) quantum numbers in several calculations. For the doubly excited states of He^- mentioned above we investigate one resonance and find that it cannot be assigned DESB quantum numbers unambiguously. We also investigate these quantum numbers for states of ^1S even parity in He. We find two types of mixing of DESB states in the doubly excited states calculated. We also show that the amount of mixing of DESB quantum numbers can be inferred from the value of the cosine of the inter-electronic angle. In a study on Li^- the calculated cosine values are used to identify doubly excited states measured in a photodetachment experiment. In particular a resonant state that violates a propensity rule is found.

To Shevek

Contents

List of Papers

I Relativistic effects on the H^- resonances converging to the $H(n = 2)$ threshold
E. Lindroth, A. Bürgers and N. Brandefelt, Phys. Rev. A **57**, R685 (1998)

II The interelectronic angle in doubly excited states and the quality of approximate quantum numbers
A. Bürgers, N. Brandefelt and E. Lindroth, J. Phys. B **31**, 3181 (1998)

III ^4S resonances of He^- below the $He^+(n = 1)$ threshold
N. Brandefelt and E. Lindroth, Phys. Rev. A **59**, 2691 (1999)

IV Strongly correlated states in the Li^- ion
G. Haeffler, I.Y. Kiyan, U. Berzinsh, D. Hanstorp, N. Brandefelt, E. Lindroth and D.J. Pegg, Phys. Rev. A **63**, 053409 (2001)

V Triply excited ^4S resonances of He^-
N. Brandefelt and E. Lindroth, submitted to Phys. Rev. A

Chapter 1

Introduction

This thesis is concerned with resonant states in atomic systems and specifically in negative ions. A resonant state is a state where more than one electron in an atom or ion is excited, and the energy of this state is enough to free one electron from the atom or ion. Our interest can be divided into two parts: resonant states as an important physical phenomena and resonant states as a good test case for how well we can describe electron correlation. They serve well as test-cases, because correlation is very strong between the excited electrons. In negative ions the electron correlation is extra strong, but there are also other reasons that makes negative ions an interesting case. Until recently the main interest has been in resonant states where two electrons are excited, doubly excited states, but lately there has been an increasing interest also in resonant states where three electrons are excited, triply excited states. The main achievement of this thesis is the development of a calculational approach that can handle triply excited resonant states.

A resonance is a very fundamental phenomenon in nature. In physics it is first encountered in the elementary mechanics course. It is described as a great increase in the amplitude of oscillation when a system is driven at a certain frequency, its resonance or natural frequency. Consider a body attached to a spring. Its natural frequency is given by the mass of the body and the spring constant ($\omega_0 = \sqrt{k/m}$). If a time varying force, with this natural frequency, is applied to the system, the amplitude of the oscillations of the body will increase indefinitely (or until the spring breaks). In atomic physics a similar matching of frequencies causes drastic effects and is the basis of the whole field of spectroscopy. If we shine light through an atomic gas we will see that the amount of absorbed or scattered light does not vary smoothly with frequency. Instead we see sharp lines in absorption spectra. In atomic theory these lines are explained with the existence of excited states in the atom. When the energy of a photon matches the energy difference of the ground state and an excited state the probability for absorption increases dramatically. An atom that absorbs a light quantum is then put in an excited state, it is excited. An excited state of an atom is normally described with one of the electrons being excited to a higher

energy level. The key word here is normally, because this thesis is about a less normal case, excited states where more than one electron is excited (i.e. multiply excited states), which can decay by sending out one or more electrons with the extra energy. Singly excited states, although they may cause resonances, are not called resonant states, but these multiply excited states are. The reason is both theoretical and experimental. A singly excited state can only decay by sending out a photon with the extra energy. If we write the Hamiltonian of the atom excluding the photon field they will be stable states, that is eigenstates to this Hamiltonian. For resonant states, that can decay by sending out an electron, there is no straightforward way to exclude all the decay channels from the Hamiltonian and calculate the resonant states as eigenstates. They are inherently unstable. This, that they can decay without interaction with something that can be seen as external to the system, is one reason why they are interesting from a theoretical point of view. The experimental reason to call these states resonant states is that they are seen as resonances in electron-impact experiments. An electron is absorbed into the atomic system, and the combined system exists for a short period of time in a multiply excited state, and then the electron is re-ejected. Although this is probably the historical reason they are called resonant states, it is not such a good reason, as the situation is not much different from the excitation of a singly excited state by a photon.

The first resonant states were observed and interpreted as multiply excited states as early as the twenties and thirties in x-ray spectroscopy, absorption spectra and scattering experiments [4, 15, 66, 8, 79, 17]. In the early sixties Fano and Cooper [20, 21] developed the well known Fano-profile parametrization of the cross-section for some excitation processes in the vicinity of an isolated resonant state. The cross section can be highly asymmetric due to constructive and destructive interference between excitation to continuum directly and via the resonant state. Madden and Codling [47] made the first observation of a doubly excited state in a photoabsorption experiment in the sixties and from then on the field expanded rapidly. Already in the same issue of Physical Review Letters Cooper, Fano, and Prats [16] made a first try to classify these doubly excited states. Later several classification schemes were developed, the most popular being the "Doubly Excited Symmetry Basis" (or the KT-quantum numbers) as developed by Herrick and Sinanoğlu [32, 69]. Even more physical insight came with the quasi-molecular quantum numbers developed by Feagin and Briggs [22, 23, 59, 60]. Also in the field of accurate calculations of resonant states there has been a great development. Nicolaides [50] distinguished three different theoretical methods: 1) methods which treat the scattering problem; 2) methods that treat the resonances as eigenstates to a non-Hermitian Hamiltonian; 3) methods that treat the resonances as ordinary bound states in the first approximation. We will not here go through the history of the development of these different methods, but only mention that the methods of this thesis fit into the second category. More background about the history and the development of the subject of resonances in negative ions and other systems can be found in Refs. [50, 65, 10].

Chapter 2

A Model Potential

Resonant states in atomic systems are quite complex. The non-relativistic Schrödinger equation is only exactly solvable for an atom with one electron, and resonant states consist of at least two excited electrons. This means that we have to solve the Schrödinger equation numerically (or by approximations) to find resonant states. Because the electron correlation is strong in resonant states it is hard to reach high accuracy. As was mentioned in the introduction resonant states can decay by sending out one or more electron. This means that as soon as we resort to a numerical basis set we have to resolve how to represent the continuum. By a continuum state we mean a state of the atomic system where one (or more) of the electrons are unbound by the potential of the nucleus. A free electron can have any kinetic energy, and the continuum is built up of all these infinitely closely spaced states. The fact that there are infinitely many of them, and that they are infinitely extended, causes some problems. Because of these complications, which will be discussed in Chapter 4, it is helpful to consider a much simpler system to understand more about the physical phenomena of resonances. This is what we will do in this chapter. We will choose a system that has resonant states but is so simple that it can be solved analytically, so that we do not have to worry about how to represent the continuum.

2.1 The Hamiltonian and its Eigenstates

In this chapter as we are only interested in the phenomena of resonances, we will use atomic units ($e = m = \hbar = 4\pi\epsilon_0 = 1$), and to make it as simple as possible we will work in one dimension. The Hamiltonian will then look like this:

$$H = -\frac{1}{2}\frac{\partial^2}{\partial x^2} + V(x). \tag{2.1}$$

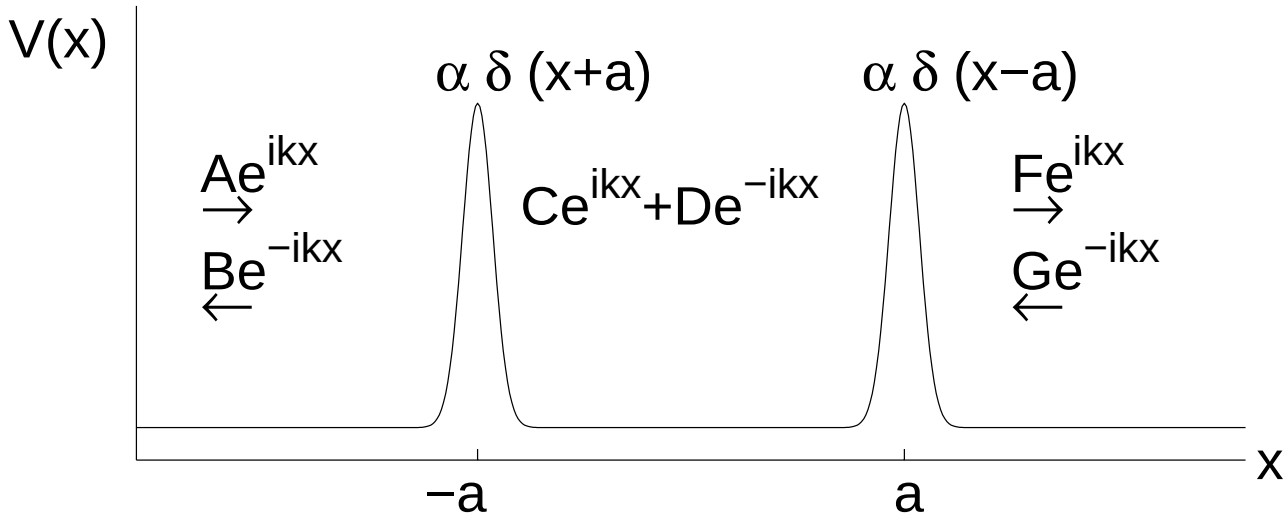

Figure 2.1: The potential with incoming and outgoing waves.

As potential we will choose two positive Dirac delta functions separated by a finite distance:

$$V(x) = \alpha\delta(x+a) + \alpha\delta(x-a), \text{with } \alpha > 0,\ a > 0, \tag{2.2}$$

where α is the strength of the potential. In this section we are interested in finding solutions to the time-independent Schrödinger equation, $H\Phi(x) = E\Phi(x)$. For our choice of potential this is very easy. The potential in each region is zero so that the solution in each region is the solution for a free particle:

$$\Phi_E(x) = \begin{cases} \Phi_I(x) = Ae^{ikx} + Be^{-ikx},\ x < -a \\ \Phi_{II}(x) = Ce^{ikx} + De^{-ikx},\ -a < x < a \\ \Phi_{III}(x) = Fe^{ikx} + Ge^{-ikx},\ x > a \end{cases}, \tag{2.3}$$

where $E = k^2/2$. See also Figure 2.1. These eigenstates are of course non-normalizable and therefore non-physical. All that is left to do is to match the wavefunction at $x = \pm a$. From the Schrödinger equation it is clear that the second derivative of the wavefunction must have a singularity of the same degree as the Dirac delta function. This means that the derivative must have a singularity of the same degree as a Heaviside step-function, and the wave function itself must be continuous. This gives us two matching conditions.

$$\Phi_I(-a) = \Phi_{II}(-a) \tag{2.4}$$

$$\Phi_{II}(a) = \Phi_{III}(a) \tag{2.5}$$

Next we have to match the first derivative of the wave function. We do this by integrating the Schrödinger equation over the two singularities at $x = -a$ and $x = a$:

$$\lim_{\epsilon \to 0^+} \int_{-a-\epsilon}^{-a+\epsilon} dx (H - E)\Phi_E(x) = 0$$

$$\Leftrightarrow -\frac{1}{2}\left(\frac{\partial}{\partial x}\Phi_{II}(x)\Big|_{-a} - \frac{\partial}{\partial x}\Phi_I(x)\Big|_{-a} \right) + \alpha \Phi_I(-a) = 0 \tag{2.6}$$

$$\lim_{\epsilon \to 0^+} \int_{a-\epsilon}^{a+\epsilon} dx (H - E)\Phi_E(x) = 0$$

$$\Leftrightarrow -\frac{1}{2}\left(\frac{\partial}{\partial x}\Phi_{III}(x)\Big|_{a} - \frac{\partial}{\partial x}\Phi_{II}(x)\Big|_{a} \right) + \alpha \Phi_{III}(a) = 0. \tag{2.7}$$

Solving these four equations for F, B, C, and D we obtain:

$$F = \frac{1}{N}\left(Ak^2 + G(-2i\alpha)(k\cos(2ika) + \alpha \sin(2ika)) \right) \tag{2.8}$$

$$B = \frac{1}{N}\left(A(-2i\alpha)(k\cos(2ika) + \alpha \sin(2ika)) + Gk^2 \right) \tag{2.9}$$

$$C = \frac{1}{N}(A(k^2 + i\alpha k) + G(-i\alpha k e^{2ika})) \tag{2.10}$$

$$D = \frac{1}{N}(A(-i\alpha k e^{2ika}) + G(k^2 + i\alpha k)) \tag{2.11}$$

$$N = k^2 + 2ik\alpha - \alpha^2 + e^{4ika}\alpha^2 \tag{2.12}$$

Equation (2.8) and Equation (2.9) give the S-matrix. This is the matrix that relates incoming and outgoing waves in time-independent scattering theory:

$$\begin{pmatrix} B \\ F \end{pmatrix} = \begin{pmatrix} S_{11} & S_{12} \\ S_{21} & S_{22} \end{pmatrix} \begin{pmatrix} A \\ G \end{pmatrix}. \tag{2.13}$$

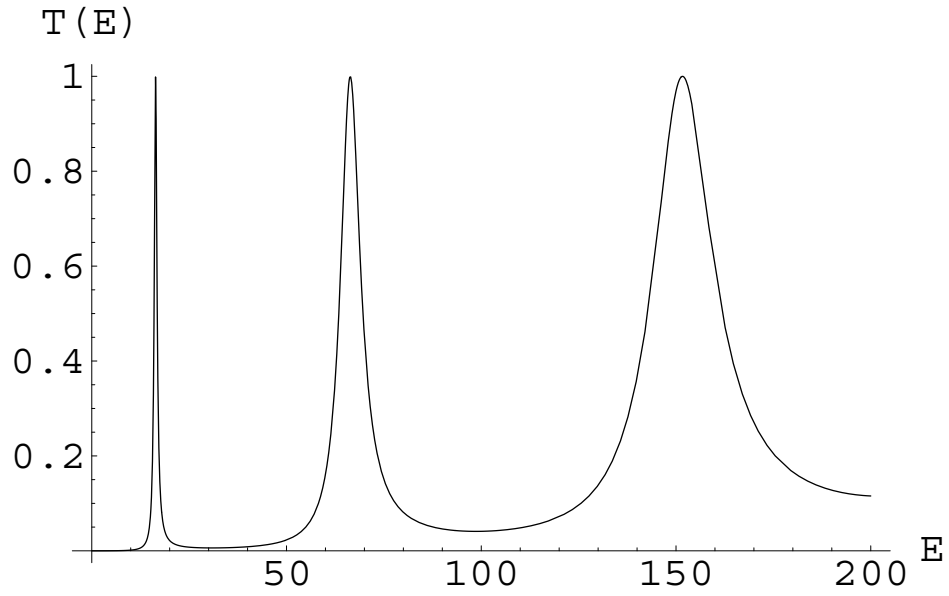

Figure 2.2: The transmission probability as a function of $E = k^2/2$ of the incoming plane wave for $\alpha = 20$ and $a = 1/4$. All numbers are given in atomic units.

2.2 Time-independent Scattering

Even though the plane wave solutions of Equation (2.3) are non-normalizable and non-physical they are quite useful. For one thing they form a complete basis set, and a physical state can be expanded in these eigenfunctions: this will be the subject of the next section. In this section we will look at *relative probabilities*. The *absolute probability* of finding a particle at a particular location is not well defined for a non-normalizable wave function, but the ratio of two probabilities is. We look at scattering of a plane wave incoming from the left. This gives us one boundary condition. There will be no incoming wave from the right and we can set $G = 0$. The *relative probability* that an incident particle is reflected is given by the reflection coefficient:

$$R = \left|\frac{B}{A}\right|^2_{G=0} = |S_{11}|^2, \tag{2.14}$$

and the probability for transmission is:

$$T = \left|\frac{F}{A}\right|^2_{G=0} = |S_{21}|^2. \tag{2.15}$$

In Figure 2.2 the transmission probability is plotted as a function of the energy of the incoming wave for $a = 1/4$ and $\alpha = 20$. The resonant behavior can clearly be seen. The S-matrix, (2.8) and (2.9), has poles whenever N (2.12) equals zero. These complex poles

correspond to the resonances. There are actually infinitely many poles for this potential. Here the first three are listed for $a = 1/4$ and $\alpha = 20$:

$$k = 5.72379 - 0.072053i,\ 11.5103 - 0.266043i,\ 17.3913 - 0.532731i, \ldots$$
$$E = 16.3783 - 0.412416i,\ 66.2082 - 3.062236i,\ 151.087 - 9.264883i, \ldots$$

It is interesting to note that, at resonance, we have 100% transmission. This is more than we would have with only one of the Dirac delta functions in the potential. A particle at resonance energy has a higher probability to pass both Dirac delta peaks than it would have to pass only one of them alone: a very non-local behavior.

We would here like to make a short detour and discuss complex scaling in relation to this model problem. In complex scaling, to be discussed in Chapter 4, the radial coordinate in three-dimensional space is rotated into the complex plane $r \to re^{i\vartheta}$. The result of this is that outgoing waves will fit in a limited cavity, that is they will approach zero as $r \to \infty$. Incoming waves will instead go to infinity as $r \to \infty$. If boundary conditions are imposed, which only allows waves which go to zero when $r \to \infty$, in the model we now discuss, this will correspond to the conditions $A = 0$ and $G = 0$ in our eigenfunction (2.3). If we now apply the four matching conditions of Equations (2.4)-(2.7) we find that we only have solutions if $N = 0$, that is when k equals the complex poles of the S-matrix ($N = 0$ has no real roots except at $k = 0$). This fact, that complex rotation gives us the poles of the S-matrix, is not so obvious but is equally true in the many electron system we will discuss later. The real part of the complex energy corresponds to the energy position and the imaginary part to the half-width of the resonance. If the resonance is broad one has to remember to exclude the background before determining the position from the transmission spectrum. If we increase α, the potential strength, the resonances will become narrower and their positions will move closer to the position of the eigenvalues of the infinite well potential. If we decrease α the resonances will become broader and start to overlap, and the energy positions will move closer to zero. In Figure 2.3, $T(k)$ is plotted for $a = 1/4$ and $\alpha = 2$. For these values the first resonance has a width comparable in size to the value of the energy. According to predictions [51, 52, 26] this would make it possible to observe non-exponential decay for long times. It would therefore be very interesting to study the explicit time-dependence. This will, however, not be done in this thesis.

2.3 Time-dependent Scattering

The time-independent formalism as used in the last section is well proven and very useful but it is not so intuitive. The scattering process is something that happens in time;

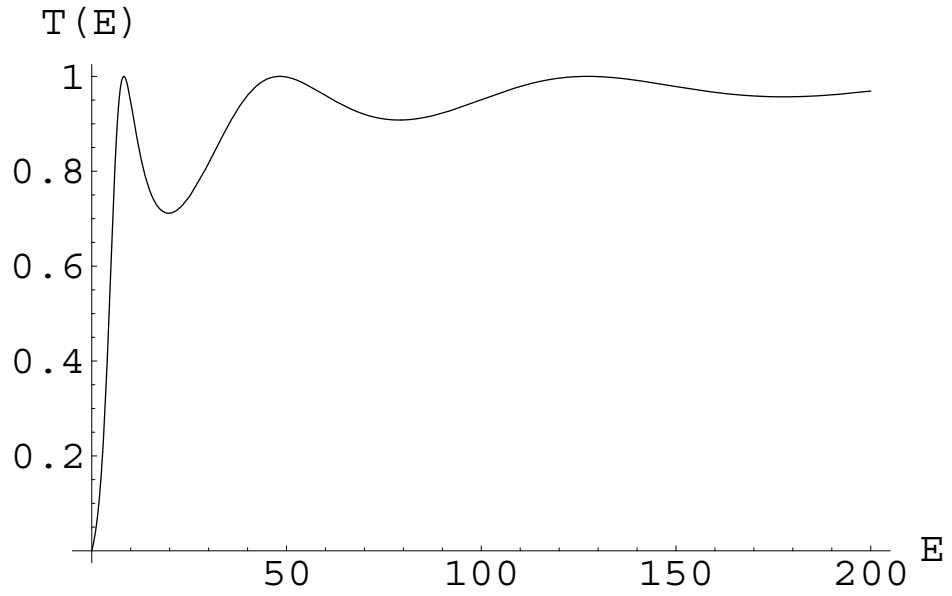

Figure 2.3: The transition probability as a function of $E = k^2/2$ of the incoming plane wave for $\alpha = 2$ and $a = 1/4$. All numbers are given in atomic units.

a particle approaches the target, interacts with the target, and is finally scattered into some direction. It would be much more direct to study this process in time. With a many electron atom or ion this is a very demanding task, but for our model potential of this chapter it is quite feasible. We start by creating a wave packet in k-space:

$$\phi(k) = \sqrt[4]{\frac{2b}{\pi}} e^{-b(k-k_0)^2 - ikx_0}, \; x_0 \ll -a, \; k_0 > 0. \tag{2.16}$$

This wave packet is centered around k_0 in k-space and around x_0 in x-space. To express it in x-space we make a Fourier transform:

$$\psi(x,0) = \frac{1}{\sqrt{2\pi}} \int_{-\infty}^{\infty} dk \phi(k) e^{ikx}. \tag{2.17}$$

The initial wave packet is now expanded in eigenstates of the free Hamiltonian. We would prefer to expand the wave packet in eigenfunctions of the actual Hamiltonian. This must be possible as they form a complete basis set. If we normalize our eigenfunctions with $A = 1$ one can see that the first term in the region $x_0 < -a$ will be the same as above. The wave packet must therefore be expanded with the same coefficients as when expanded in eigenfunctions of the free Hamiltonian. The second term must cancel as we know there exists an expansion. This holds true to the extent that the wave packet is negligible in the regions $x_0 > -a$.

$$\psi(x,0) = \frac{1}{\sqrt{2\pi}} \int_{-\infty}^{\infty} dk \phi(k) \Phi_E(x,k) \tag{2.18}$$

This scattering theorem is often used in three dimensions in textbooks on scattering theory, see for example the book by Eugen Merzbacher [48]. As the wave is incoming from the left we shall also put $G = 0$. It is now trivial to get the wave function at any later time by applying the time-translation operator:

$$\psi(x,t) = e^{-itH}\psi(x,0) = \frac{1}{\sqrt{2\pi}}\int_{-\infty}^{\infty} dk\phi(k)e^{-itk^2/2}\Phi_E(x,k). \tag{2.19}$$

The integral can be solved with for example the Mathematica program [80]. In Figure 2.4 a wave packet is plotted for different times. Note that the Dirac delta functions are very close to zero on the x-axis. We have chosen k_0 so that the wave packet is on resonance. Each time-step represents the time within which a wave packet would travel the distance of ten units if the potential was constant and equal to zero for all x. The y-axis is kept constant to give a pedagogical picture of the time evolution. The strong peak that builds up in the potential actually reaches much higher. For example at $t = 6.99$ the peak reaches 1.4. The black areas are rapid oscillations of the wave function, due to interference of the incoming wave and the reflected wave. It is clearly seen how the wave function builds up between the two Dirac delta functions and then leaks out. It leaks out mostly in the forward direction as could be seen from the transmission coefficient: a somewhat strange behavior.

If we calculate the probability to find the particle between the two Dirac delta functions as a function of time (Figure 2.5), we find that it is very dependent on the shape and extension of the wave packet. The resonant state starts to decay before it is completely created and it is thus not possible to define a t=0-state. By a t=0-state we mean a state for which we are certain that the particle is located between the Dirac delta functions. We can still calculate the decay rate if we concentrate on times when only negligible parts of the wave packet are still entering from the left. Fitting an exponential to the tail of the probability curve we find the decay rate to be 0.82. This gives us a lifetime or mean life of $\tau = 1/0.82$. From the complex pole of this resonant state we get $\Gamma = 2 * 0.41$, so the lifetime is in agreement with the time-energy uncertainty relation with an equal sign $\Delta E \Delta t = 1$. It is interesting to note that the lifetime can be calculated even though no t=0-state can be defined.

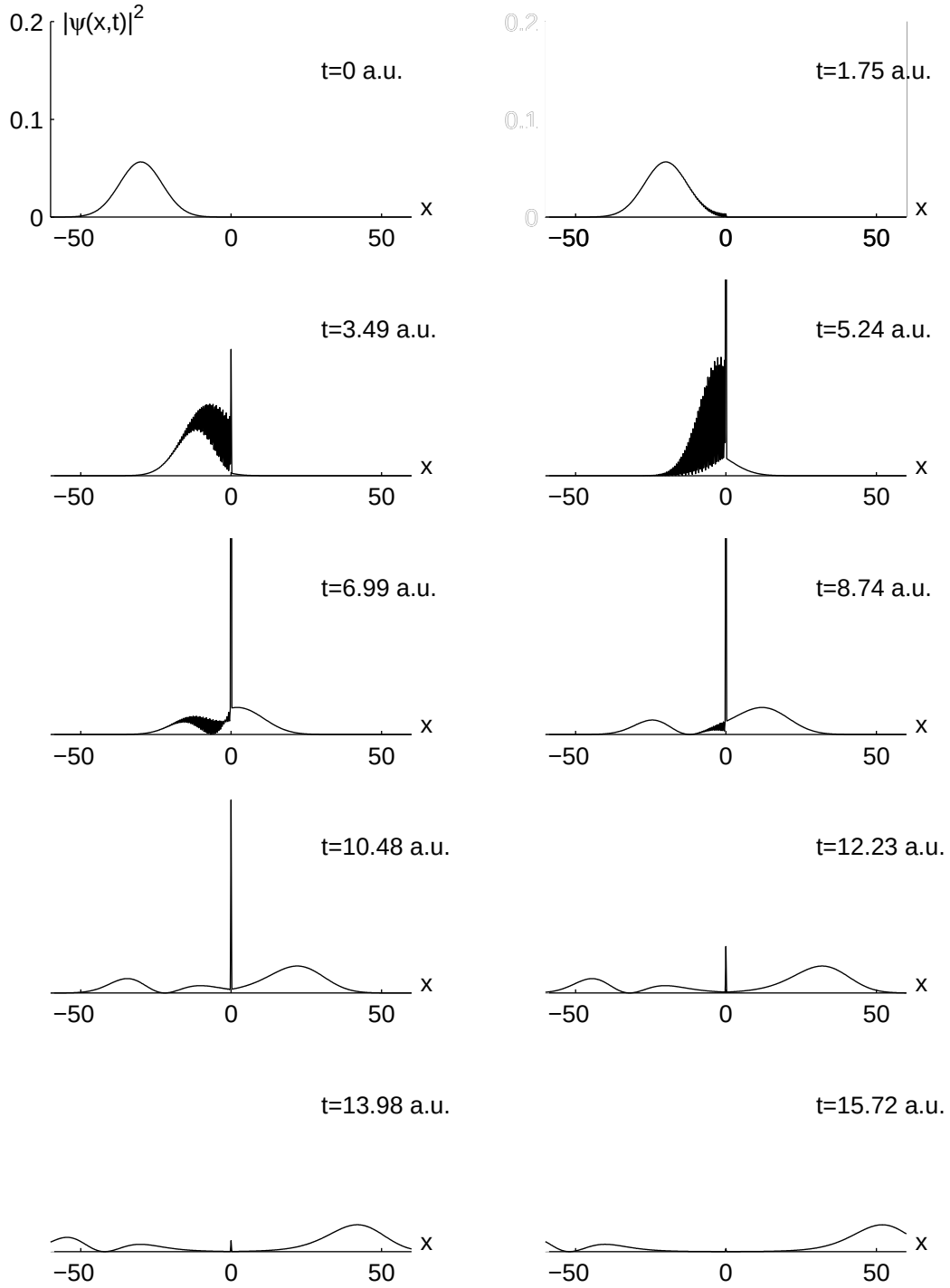

Figure 2.4: A wave incoming from the left is plotted for different times. $x_0 = -30$, $k_0 = 5.72379$, and $b = 50$ are used. The potential is set to $a = 1/2$ and $\alpha = 20$, so the extension of the potential is very small compared to the extension of the wave. The y-axis is the same for all plots. All numbers are given in atomic units.

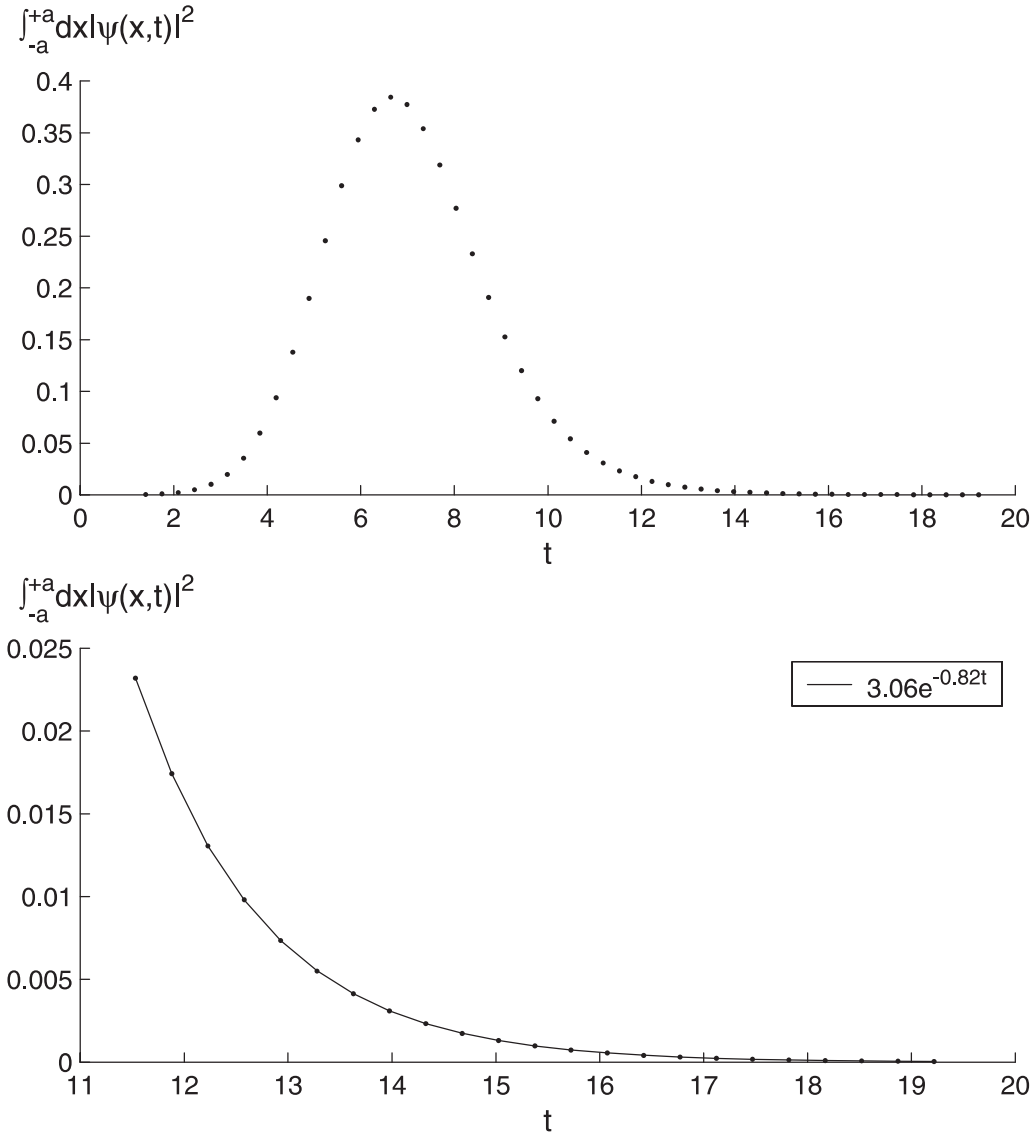

Figure 2.5: The probability to find the particle inside the potential as a function of time. For large t this can be seen as the survival probability of the resonant state. An exponential curve is fitted, and the mean life is found to be $1/0.82$. All numbers are given in atomic units.

Chapter 3

Multiply Excited States

A doubly excited state is a state where two electrons have been excited to higher energy levels. In a two electron system (e.g. H^-, He, Li^+,...,) such a state will always be situated above the first ionization threshold, i.e. it takes more energy to excite both electrons to the next level than it takes to free one electron from the atom. For other many-electron systems, doubly excited states can be situated both above and below the ionization threshold. In this thesis we are only concerned with states above the ionization threshold. Such states are also called pseudo-states, resonant states, and resonances. A state above the ionization threshold is degenerate with a continuum state, a state where one of the electrons is free, and it can decay via interaction with this continuum state. In atoms this is called autoionization, because the atom emits one electron and becomes ionized. A doubly excited state can also decay by sending out a photon, but for low nuclear charge this is much less likely. If the system to begin with is not an atom but a negative ion, a doubly excited state that sends out one electron will leave the system neutral and is instead called autodetaching. In a three-electron system we also have the possibility to create triply excited states. In Figure 3.1 a schematic drawing of the energy levels of a three-electron system is shown. As can be seen, the first triply excited state is situated above the first double ionization threshold, so that it can emit both one and two electrons. This sketch is drawn neglecting electron-electron interaction so that only the principal quantum number n determines the energy. When the electron-electron interaction is included the energy will also depend on the angular momentum of the electrons. We will then have different series of resonances for different total angular momentum L, total spin S, and parity π. See Section 3.2 for an example.

Multiply excited states can be excited in any process that transfers energy to the atomic system. In for example photoabsorption, an incident photon can excite the system into a multiply excited state, which then de-excites by sending out an electron (with high probability). This process has the same initial and final states as direct excitation of the electron into the continuum, and the two processes will interfere to produce asymmetric

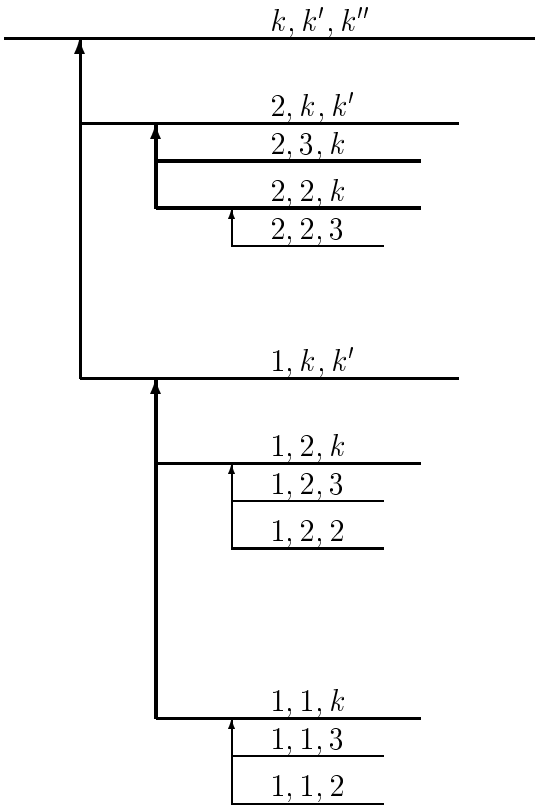

Figure 3.1: A schematic three electron system energy level diagram. On each level n_1, n_2, and n_3 is given. At each threshold electrons that have escaped are represented with the wave number (k).

profiles in the absorption spectrum. Photoabsorption experiments are of direct interest in this thesis, in paper I [5], in paper III [39, 40, 38], and in paper IV. Multiply excited states are also observed in particle-atom collision experiments, beam-foil experiments, and atom-surface collisions to mention a few, and they are very important in many charge transfer processes in collisions. Often in these latter cases the multiply excited states are not resonances but discrete states below the ionization threshold.

The asymmetric profiles in the cross section due to resonant states are usually called Fano profiles. In two papers Fano and Cooper [20, 21] investigated the shape of these. They found that the effect on the background, due to an isolated resonant state, can be described by the energy position, the width, and a shape parameter:

$$\sigma(q, \varepsilon) = \sigma_0 \frac{(q + \varepsilon)^2}{1 + \varepsilon^2}, \tag{3.1}$$

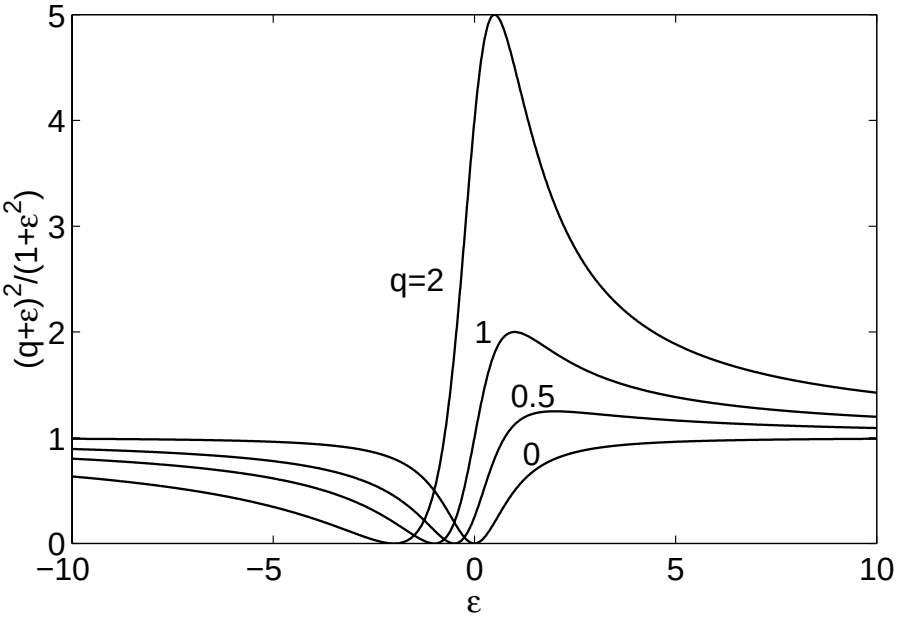

Figure 3.2: Fano profiles for different values of the shape factor q.

where q is the shape parameter and ε is defined by:

$$\varepsilon = \frac{\hbar\omega - (E_r - E_0)}{\Gamma/2}. \tag{3.2}$$

E_r is the resonance energy position, E_0 is the energy position of the state from which the system is excited, and Γ is the width of the resonance. In Figure 3.2 we have plotted profiles for different values of q. As q increases the profile looks more and more like a symmetrical Lorentz profile. For $q = 0$ a symmetrical dip in the cross section is obtained. Such a resonance is called a window resonance. For other values of q the profile is asymmetric.

3.1 Negative Ions and the Special Case of H^-

Negative ions are fundamentally different from neutral atoms or positive ions. In a neutral atom or a positive ion the outermost electron sees a positively charged ion core. The main interaction is then the long range Coulomb interaction. We then get an infinite number of singly excited states converging as $1/n^2$ to the first ionization threshold, a so called Rydberg series. There is also an infinite number of doubly excited states also converging as $1/n^2$ to the higher thresholds. In a negative ion the outer electron sees no net charge but experiences the field from an induced dipole, and there is only a finite number of

bound states or in some cases no bound states at all. The number of doubly excited states converging to each threshold is also limited. A special case is H^-. The energy levels of a one-electron system are degenerate with respect to angular momentum in a non-relativistic picture. This leads to the well known linear Stark effect in hydrogen-like systems; i.e. that the energy splitting caused by an electric field is linear with respect to the field strength. In a general atom the Stark effect is quadratic. The same effect causes the outer electron in H^- to experience an attractive dipolar potential proportional to $1/r^2$ as $r \to \infty$. In a general negative ion the dipolar potential decays as $1/r^4$. Gailitis and Damburg [24] show that if a $1/r^2$ potential is sufficiently attractive infinite series of resonances, converging exponentially to all thresholds are expected, i.e.

$$R = \frac{\epsilon_N}{\epsilon_{N+1}}, \tag{3.3}$$

where ϵ is the energy relative to the threshold, R is a constant that can be calculated from the asymptotic Hamiltonian, and N counts the resonances. This convergence is investigated for ${}^1P^o$ symmetry in H^- below the H($n = 2$) threshold in paper I.

3.2 Alternative Quantum Numbers

The independent-particle model cannot describe doubly excited states even qualitatively because of the importance of electron-electron repulsion in these states. Already in the sixties Cooper, Fano, and Prats [16] realized that the measurements of doubly excited states in He by Madden and Codling [47] could not be interpreted in the independent particle model. This was the first observation of photoexcited doubly excited states. Madden and Codling used synchrotron radiation to excite He from the ground state to doubly excited states below the He(n=2) threshold. It was clear that they could only reach states of ${}^1P^o$ symmetry, but how could they be further classified? ${}^1P^o$ is to be understood as ${}^{2S+1}L^\pi$, where S is the total spin, L is the total angular momentum, and π is the parity. For parity o means odd parity, $\pi = -1$, and e means even parity, $\pi = +1$. Because the threshold is degenerate ($He^+(2s)$ and $He^+(2p)$ have the same energy) we expect three series converging to this threshold. In the independent particle picture we would classify them as $2snp$, $2pns$ and $2pnd$. Of these only $2snp$ and $2pns$ would be excited from the ground state. Cooper, Fano, and Prats suggested that the electron-electron repulsion would mix these two series into a plus and a minus series: $2snp + 2pns$, $2snp - 2pns$. They also suggested a propensity rule: the optical transition from the ground state to the minus levels is quasi-forbidden. This could then explain why only one series (the plus series) was seen in the experiment. Later several classification schemes were suggested. The aim was to understand why resonances with the same total symmetry have such different characteristics. The first and still most popular classification scheme

was the group-theoretical approach by Wulfman and Sukeyuki [81], and Sinanoğlu and Herrick [69]. This classification scheme, called the Doubly Excited Symmetry Basis, was thoroughly examined by Herrick and coworkers [32, 28, 30, 31, 37] and the results were summarized in Ref. [29]. Another more physically intuitive classification scheme is the molecular orbital approach by Feagin and Briggs [22, 23]. This scheme was further investigated in Refs. [59, 60, 61, 62]. It has been shown that the molecular orbital quantum numbers contain and explain the DESB quantum numbers (see paper II). In this section we will use the more popular DESB classification.

In general in a two-electron atom there are several series converging to each threshold for a specific symmetry $^{2S+1}L^{\pi}$. If electron correlation were absent each series could be labeled with the l values of the electrons. The n value of the inner electron would be fixed by the threshold towards which the series converges, and the n value of the outer electron would count the different doubly excited states, increasing towards the threshold. Keeping with the custom of many authors we will use N for the inner electron and n for the outer electron. When electron correlation is included L, M_L, S, M_S, and π are still good quantum numbers, but the n and l values of the two electrons are not. We can therefore no longer use the l values to classify the different series. The idea of the DESB approach is to exchange l_1 and l_2 with two new approximately good quantum numbers. For the change from the l_1, l_2 basis to the DESB basis see Section 4.2.1. The new quantum numbers are called K and T and they can take the following values:

$$T = 0, 1, ..., \min(L, n_1 - 1), \tag{3.4}$$

$$K = -(n_1 - T - 1), -(n_1 - T - 1) + 2, ..., n_1 - T - 1. \tag{3.5}$$

Different series below a specific threshold (N) can now be classified with K and T, and a specific state within a series would be classified with n, K, and T. The n-value of the inner electron, N, is asymptotically a good quantum number as the outer electron is excited farther and farther out. For the state that makes up the threshold it is perfectly good. The n-value of the outer electron, n, is usually not such a good quantum number. It is sometimes exchanged for some effective quantum number (see paper II) or some ordering number (see paper IV). The new quantum numbers can be understood as follows. T is proportional to the quantization of $\mathbf{L} \cdot \mathbf{B}$, where $\mathbf{B} = \mathbf{b}_1 - \mathbf{b}_2$. The vectors $\mathbf{b}_1$ and $\mathbf{b}_2$ are the Runge-Lenz vectors of the electrons. The exact relation is [9]:

$$(\mathbf{B} \cdot \mathbf{L})^2 |NnKTL^{\pi}\rangle = (K + n)^2 T^2 \hbar^4 |NnKTL^{\pi}\rangle. \tag{3.6}$$

The K quantum number can be related to the expectation value of $\cos\theta_{12}$, where θ_{12} is the angle between the two electrons [29]:

$$\langle \cos\theta_{12} \rangle = -\frac{K}{N} + \frac{N^2 - 1 - K^2 - T^2 + 2\mathbf{l}_1 \cdot \mathbf{l}_2/\hbar^2}{2Nn} \tag{3.7}$$

If n is much larger than N, $\langle \cos\theta_{12} \rangle \approx -K/N$. This means that the highest possible K corresponds to the electrons on different sides of the nucleus, K equal to zero corresponds to an angle of 90° between the electrons, and a negative K value corresponds to the electrons on the same side of the nucleus. This is why negative K-values are not expected for negative ions, where the repulsion would be too great compared to the weak attraction from the core.

To describe the radial correlation a new quantum number was introduced [29]. This quantum number was called A by Lin and can take the values +1, 0, and −1 [41, 42]. It is completely determined by the quantum numbers already introduced:

$$A = \pi(-1)^{S+T} \text{ if } K > (L-N), \quad A = 0 \text{ otherwise} \tag{3.8}$$

For $A = +1$ the wavefunction has an antinode at $r_1 = r_2$, for $A = -1$ it has a node, and for $A = 0$ it is highly asymmetric with one electron close to the nucleus and one far away and there is little radial correlation [78].

Kellman and Herrick also investigated the vibrational structure [37]. This led to yet another quantum number n_ν or ν. We use here the definition from Watanabe and Lin in Ref. [78]:

$$n_\nu = \frac{1}{2}(N - K - T - 1). \tag{3.9}$$

n_ν is the number of nodes in the θ_{12} coordinate.

With the help of the new quantum numbers not only can the structure of the doubly excited states be understood but also the differences in width between different doubly excited states, the autoionization and radiation rates to different channels, and the photoexcitation strengths to different states. There are propensity rules for both autoionization and photoexcitation [59, 75, 60, 63, 25]. Selection rules tell us which transitions are allowed. Already in the beginning of this section when we discussed the experiment by Madden and Codling [47] we used selection rules for photoexcitation. These were the usual rules that apply to a simple one-electron atom. When a photon is absorbed, parity must change, $\pi \rightarrow -\pi$, the l value must change by one unit, $l \rightarrow l \pm 1$, and the spin is unchanged, $s \rightarrow s$. Translated to a two-electron atom these rules mean that the total parity must change, $\pi \rightarrow -\pi$, the total angular momentum can change, $L \rightarrow L+1, 0, -1$ (not $0 \rightarrow 0$), and the total spin is unchanged, $S \rightarrow S$. Propensity rules on the other hand try to explain why some states give rise to prominent resonances and some can hardly be seen although they are allowed according to the selection rules. In this thesis we will only mention the propensity rules for photoexcitation as presented by Sadeghpour and Greene

[63]. In ref. [63] they use measurements of Harris *et al.* [27] of high lying ${}^1P^o(N = 3 - 8)$ resonances in H^-, to find the propensity rules:

$$\Delta A = 0,\ \Delta n_\nu = 0 \tag{3.10}$$

($\Delta A = 0$ was actually suggested earlier by Cooper, Fano, and Prats [16]). This propensity rule is investigated in paper IV. A more general propensity rule can be found in Ref. [75].

Chapter 4

Methods

In this chapter we discuss the different methods used in this thesis. Before we embark on the different details we give an overview of the procedure. The aim of our methods is to solve the two- or three- electron non-relativistic Schrödinger equation. This is done by diagonalization of the Hamiltonian with a complete basis set in a limited spherical cavity. As a basis set we use coupled eigenfunctions of the one-electron Hamiltonian. By a limited cavity we mean that we force the eigenfunctions to be zero at a certain distance from the origin. If the electron-electron repulsion was neglected our coupled eigenfunctions would be eigenfunctions of the two- or three- electron Hamiltonian. The repulsion term(s) will now mix these basis functions, but the total angular momentum, L, the total spin, S, and the parity, π, will still be good quantum numbers even with the repulsion term(s) included. That is the reason we use coupled eigenfunctions: it allow us to solve for one total symmetry, ${}^{2S+1}L^{\pi}$, at a time. If we did not solve for one symmetry at a time the problem would be much too big. All angular integrals are performed analytically using Racah algebra [43]. The radial coordinate, however, has to be represented numerically. In some cases we use a discretized grid [64] and in some we use B splines [18]. We are mainly interested in calculating auto-detaching states. To describe these states, we need to describe states where one or two electrons are unbound by the nucleus. These electrons can have any kinetic energy and these states are called continuum states. Continuum states are not square integrable and we use complex rotation to represent these in a limited cavity [1]. In the first article presented in this thesis we consider some relativistic corrections. All other calculations are done non-relativistically. In article number four we work with a potential from a $1s^2$ core. In all other cases the one-particle potential used is a simple Coulomb potential. In the first section we describe how we diagonalize the one-electron Hamiltonian to get our basis set, in the second we describe how we use this basis set to diagonalize the two-electron Hamiltonian, and in the third we mention some things that are specific for the three-electron problem.

4.1 One Electron

As mentioned above we want to use coupled eigenfunctions of the one-electron Hamiltonian to solve the two- or three-electron Hamiltonian in a limited spherical cavity for one symmetry, $^{2S+1}L^{\pi}$, at a time. The angular parts of the matrix elements in the two- or three-electron Hamiltonian can be calculated analytically so we only need to solve numerically for the radial coordinate. Coupling the angular momentum and spin of the electrons has nothing to do with the radial coordinate, so the radial functions in our basis set do not need to be eigenfunctions of the one-electron Hamiltonian. Any radial basis functions will do. There are however some good reasons for solving the radial one-electron problem and using eigenfunctions of the one-electron Hamiltonian as basis functions. One reason is that we can inspect the radial one-electron eigenfunctions and eigenvalues to get an idea of what the chosen numerical representation of the radial coordinate can and cannot describe. Another, even more important reason is that the eigenfunctions with highest principal quantum number n, (that is, with highest energy) can be excluded from the final diagonalization of the two- or three-electron Hamiltonian without affecting the position or width of the resonances of interest. If we use a discretized grid to represent the radial coordinate (Section 4.1.1) a typical number of points used is seventy. We then get seventy one-electron eigenfunctions for each l-value. It might then be possible to exclude as many as half of them including eigenfunctions only up to $n = 35$ when we build our coupled basis set. This makes the final matrix to be diagonalized much smaller. If we use B splines (Section 4.1.2) to represent the radial coordinate we use typically twenty B splines. It is then possible to exclude one to three eigenfunctions. When we are diagonalizing the three-electron Hamiltonian the size grows very rapidly with the number of one-electron eigenfunctions so that the exclusion of these eigenfunctions from the basis set can be crucial. Yet another good reason is that we can examine the eigenfunctions of the many-electron Hamiltonian to find how it is built up by one-electron eigenfunctions. For example a resonance may be built up almost completely from eigenfunctions where one electron is in $1s$. In such a case it might also be possible to use only eigenfunctions where one electron is in $1s$ to test different aspects of the calculations. This is done in paper III. It is also because we use these one-electron solutions that we can translate our expansion of our resonance eigenfunctions in hydrogen-like eigenfunctions to an expansion in DESB eigenfunctions so easily (Section 4.2.1). There is also another case where it would be very awkward not to diagonalize the radial one-electron Hamiltonian. That is where we want to have a potential that includes the effect of core electrons (Section 4.1.3).

There are thus good reasons to diagonalize the radial one-electron Hamiltonian, and it is now time to look at how it will be done. We will separate the one-particle wave function as follows:

$$\psi(r,\theta,\phi) = \frac{P(r)}{r} Y_m^l(\theta,\phi). \tag{4.1}$$

The radial Schrödinger equation in SI units reads then:

$$\left[-\frac{\hbar^2}{2\mu}\left(\frac{d^2}{dr^2}-\frac{l(l+1)}{r^2}\right)-\frac{Ze^2}{4\pi\epsilon_0 r}\right]P(r)=\epsilon P(r), \tag{4.2}$$

where $\mu = mM/(m+M)$ is the reduced mass of the electron. To ensure a finite wave function at $r = 0$, we require $P(r) \to 0$ as $r \to 0$, and to have a normalizable wave function we also require $P(r) \to 0$ as $r \to \infty$. We will actually use a limited cavity with $P(R) = 0$ for some R large enough not to affect the states of interest. There will be two kinds of solutions, states bound by the potential with negative eigenvalues and states bound by the cavity with positive eigenvalues. The states bound in the potential with the highest energy will be affected by the cavity and not be so hydrogen-like, and the states with the lowest energy will hardly be affected by the cavity wall at all. The states with positive eigenvalues will represent the continuum of a free electron (more about this in Section 4.1.4).

4.1.1 Discretized Grid

In this method [64] the Schrödinger equation (4.2) is converted into a matrix equation, $H\mathbf{P} = \epsilon\mathbf{P}$, where the elements of the vector $\mathbf{P}$ are the values of the eigenfunction at the discretized points of r. To represent r, we use an exponential lattice, instead of a linear lattice, because the eigenfunctions we want to represent go to zero exponentially for large r. The grid points are set at $r = e^x$, for equidistant x. To preserve hermiticity of the differential operator when discretized we make the transformation:

$$P(r) \to \frac{1}{\sqrt{r}}P(x) \tag{4.3}$$

To express the second derivative in the Hamiltonian we use a symmetric five-point formula:

$$\begin{aligned}&\frac{d^2}{dx^2}y(x) \\ &= \frac{1}{12h^2}\left[-y(x-2h)+16y(x-h)-30yx+16y(x+h)-y(x+2h)\right]+O(h^4),\end{aligned} \tag{4.4}$$

which gives us a symmetric eigenvalue problem. To calculate the derivative close to the boundary, points outside the lattice are needed. Beyond the last lattice point $P(r)$ is

assumed zero, and close to the nucleus $P(r)$ is approximated by:

$$P(r) \propto r^{l+3/2}\left(1 - \frac{Zr}{l+1}\right) \tag{4.5}$$

When taking care of the boundary it is important to keep the matrix symmetric. This is accomplished by using:

$$P(x_0) = \alpha\frac{P(x_0)}{P(x_1)}P(x_1) + (1-\alpha)\frac{P(x_0)}{P(x_2)}P(x_2),\ P(x_{-1}) = \frac{P(x_{-1})}{P(x_1)}P(x_1), \tag{4.6}$$

and adjusting α appropriately. The ratios are calculated from Equation (4.5). This approach has been used in paper I and in paper II.

4.1.2 B splines

Especially when we want to solve a three-electron problem it is very important to keep the number of one-electron eigenfunctions to a minimum. It is then better to use B splines than a discretized grid. For a complete introduction to B splines we recommend the excellent book by de Boor [18]. To construct B splines, a set of points $\{t_i\}$ called the knot set is defined on a given interval, in our case $[0, R]$, where R is the size of the cavity. The only necessary restriction on the knot set is that $t_i \leq t_{i+1}$. B splines of order k are defined recursively as follows:

$$B_{i,1}(x) = \begin{cases} 1 & \text{if } t_i \leq x < t_{i+1} \\ 0 & \text{otherwise} \end{cases}, \tag{4.7}$$

$$B_{i,k}(x) = \frac{x - t_i}{t_{i+k-1} - t_i}B_{i,k-1}(x) + \frac{t_{i+k} - x}{t_{i+k} - t_{i+1}}B_{i+1,k-1}(x). \tag{4.8}$$

B splines are non-zero from the i:th knot point to the $(i+1+k)$:th knot point, that is, on k intervals. They are piecewise polynomials of degree $k-1$. We will need the derivative of a $B_{i,k}$ spline. It is easily expressed as a sum of two B splines of one order lower, $k-1$:

$$\frac{d}{dx}B_{i,k}(x) = \frac{-k+1}{t_{i+k} - t_{i+1}}B_{i+1,k-1}(x) + \frac{k-1}{t_{i+k-1} - t_i}B_{i,k-1}(x) \tag{4.9}$$

By using multiple knot points we can introduce discontinuities where needed. The $(k - m)$th derivative is the first discontinuous derivative in an m-fold multiple knot point.

To transform Equation (4.2) to a symmetric generalized eigenvalue equation we follow the standard procedure. $P(r)$ is expanded in B splines, $P(r) = \sum c_i B_{i,k}(r)$. We multiply both sides of Equation (4.2) with $B_{j,k}(r)$, and integrate over r. The result will be a generalized eigenvalue equation, because the B splines are not orthogonal to each other if they are of order greater than one. Note also that the symmetric form is guaranteed by the boundary conditions in $r = 0$ and $r = R$.

$$\mathbf{hc} = \epsilon \mathbf{Bc} \tag{4.10}$$

$$h_{ji} = \langle B_{j,k}|h(r)|B_{i,k}\rangle,\ B_{ji} = \langle B_{j,k}|B_{i,k}\rangle \tag{4.11}$$

The freedom of the knot-point distribution which defines the splines of a given order is a great advantage which we explore, but we will always put k knots at $r = 0$ and $r = R$. All other knot points appear only once. The first and last spline will be removed from the basis set. These are the only splines which are non-zero at $r = 0$ and at $r = R$, and by removing them the boundary conditions $P(0) = P(R) = 0$ are enforced. This is the same scheme as used by Johnson *et al.* [35, 36], who pioneered the use of B splines in atomic calculations. Another possible boundary condition is to put only one point at $r = R$. This would force the eigenfunctions to approach zero smoothly for large r. This is always true for the states we are interested in, because we are interested in states that are not affected by the non-physical cavity wall. Such states have to go to zero before reaching the cavity wall. With this scheme it should be possible to use fewer B splines than with the conventional scheme. Some tests were done when calculating He^- and the results looked promising, but the tests were never completed due to lack of time. Therefore this scheme is not used in any of the calculations presented in this thesis.

When placing the knots we use three regions. In the first region we place them equidistantly. This is the region where the resonant state is large in the final many-electron calculation. In region two we distribute the knots exponentially. This is where the resonant state is approaching zero exponentially. Finally in region three we have no knot points except on the boundary. In this region the localized part of the resonant state is negligible, but we need it to represent the non-localized part of the state, the continuum of one free electron. To integrate the B splines we use Gaussian quadrature, which can be done to machine accuracy if necessary. As an example of a B spline basis we will look at the knot sequence used to calculate the first resonance presented in paper III, a doubly excited state of He^-. We use atomic units, $e = m = \hbar = 4\pi\epsilon_0 = 1$ and do the calculation for infinite mass of the nucleus. B splines of order $k = 5$ are used as in all calculations presented in this thesis. The knot points are distributed linearly up to

0.6 a.u. and exponentially from 0.6 a.u. to 58.9 a.u. and then there are no more knot points until the cavity boundary at 200 a.u. A total of 28 knot points is used resulting in 21 B splines. The eigenvalues for $l = 0$ are presented in Table 4.1. As can be seen the description is quite good although we only have 21 B splines: for $n = 1$ we have seven correct figures. Deviations from the analytical value depend both on the limited number of B splines and on the cavity wall. B splines are used in paper III, IV, and V.

4.1.3 $1s$ Core

In paper IV of this thesis we calculate resonances in Li^-. This is done by treating Li^- as two electrons outside a core consisting of the nucleus and two $1s$ electrons. The closed $1s$ shell is then treated as a frozen shell using the Hartree-Fock method. The procedure will be outlined below. For a complete treatment of the Hartree-Fock method the book by I. Lindgren and J. Morrison [43] is recommended. To the Hamiltonian (4.2) a non-local spherically symmetric potential, $u_{HF}(r)$, is added that will give the potential from the mean field of the two core electrons. The two core electrons themselves are calculated in this mean field and are not in the first approximation affected by the two outer electrons. This is what is meant by frozen core and it will be a good approximation for highly excited doubly excited states. For further corrections to this approximation please see Ref. [45]. The effect of $u_{HF}(r)$ operating on a function of r for a specific l-value, $l = l_a$, is defined by [43]:

$$u_{HF}(r)B_i(r) = \frac{e^2}{4\pi\epsilon_0}\left(2\int_0^\infty dr' \frac{1}{r_>}P_{1s}(r')^2 B_i(r) - \frac{1}{2l_a+1}\int_0^\infty dr' \frac{r_<^{l_a}}{r_>^{l_a+1}} B_i(r')P_{1s}(r')P_{1s}(r)\right), \tag{4.12}$$

where $r_>$ and $r_<$ is the greater and lesser of r and r', respectively. As can be seen the value at a specific r depends on the value of $B_i(r)$ for all r, i.e. the potential is non-local. Another complication is that it depends on the $1s$ eigenfunction. This means that we have to solve iteratively to find the solutions for $l = s$. We can start with the eigenfunctions of the Hamiltonian without $u_{HF}(r)$ as our zeroth order solution and then solve for the next order. This procedure is then continued until the difference in eigenvalue for the $1s$-eigenfunction for two different orders is below some small value. We also check that the norm $|\langle P_{1s}^{o+1}|P_{1s}^{o}\rangle|^2$ is close to one (o is the order of iteration). When the $l = s$ spectrum is calculated the other l-values can be solved for directly.

Table 4.1: Eigenvalues to the radial one-electron Schrödinger equation for $l = 0$ obtained with 21 B splines defined with the same knot sequence as used to calculate the first resonance in paper III of this thesis, a resonance of $^4S^e$ symmetry in He^-. The analytic values are also given for comparison.

n	numerical (a.u.)	analytical (a.u.)
1	-1.999999801	-2.000000000
2	-0.499999538	-0.500000000
3	-0.222220588	-0.222222222
4	-0.124994074	-0.125000000
5	-0.079978185	-0.080000000
6	-0.055469345	-0.055555556
7	-0.039889971	-0.040816327
8	-0.027308077	-0.031250000
9	-0.022145365	-0.024691358
10	-0.015593013	-0.020000000
11	-0.010909500	-0.016528926
12	0.058755821	
13	0.314252303	
14	0.934907662	
15	2.291462442	
16	5.081852990	
17	10.609858518	
18	21.315791145	
19	41.768326712	
20	83.526719249	
21	261.844196925	

4.1.4 Complex Rotation

The aim of our methods is to calculate resonant states in many-electron systems. As was mentioned in Chapter 3 these states can decay by emitting one or more electrons with the extra energy. This means that we have to be able to describe the continuum of free

electrons. To do this in a limited cavity we use the method of complex rotation. This method, also known as complex scaling, complex coordinates, coordinate rotation, and dilatation analyticity, was developed in a number of papers: Aguilar and Combes [2], Balslev and Combes [7], Simon [67, 68] and van Winter [74]. It allows a resonant state to be calculated as a bound square-integrable state of a complex rotated Hamiltonian with a complex eigenvalue (Section 4.2.3). In this thesis different aspects of complex rotation will be examined, but for a more theoretical background see Ref. [1] and references therein.

In this section we will look at the effect on the one-electron spectrum only. In the complex rotation method the radial coordinate is rotated into the complex plane, $r \to re^{i\vartheta}$. The radial Schrödinger equation will then be:

$$h(re^{i\vartheta})P(re^{i\vartheta}) = EP(re^{i\vartheta}). \tag{4.13}$$

Sofar we have only made a variable substitution. What makes this interesting is the boundary conditions. We will still look for solutions for which $P(R) = 0$, rather than $P(Re^{i\vartheta}) = 0$. Not all solutions to the unrotated equation that fulfill $P(R) = 0$ will, when rotated $P(r) \to P(re^{i\vartheta})$, still fulfill $P(r = R) = 0$, as this will require that $P(R) = P(Re^{i\vartheta})$. For solutions that die off exponentially for large r it will be true as can easily be seen. So the hydrogen-like solutions to the unrotated Hamiltonian will be solutions to the rotated Hamiltonian with the same eigenvalues, just let $P(r) \to P(re^{i\vartheta})$. Our positive energy solutions, however, do not die off exponentially. These are solutions which are eigenstates of the cavity and for large r they are proportional to $\sin(kr)$. For the unrotated equation we get solutions for k that fulfill $\sin(kR) = 0$. This means that we get eigenvalues $E = \hbar^2 k^2/2\mu$. For the rotated equation $R \to Re^{i\vartheta}$, and we get solutions for $ke^{-i\vartheta}$ instead. The eigenvalues will then be $Ee^{-2i\vartheta}$, i.e. the solutions in the cavity (those with positive energy) will be rotated 2ϑ into the complex plane. These states represent a pseudo-continuum and will be called continuum states. They represent a pseudo-continuum rather than a true continuum not only because they are discretized so that there are only a finite number of states, but also because they represent only an outgoing wave. This is enough for us to be able to represent our resonant states. To see that they represent an outgoing wave it is easiest to complex-rotate an outgoing wave:

$$\frac{e^{ikr}}{r} \to \frac{e^{ikre^{i\vartheta}}}{re^{i\vartheta}} = \frac{e^{ikr\cos\vartheta}e^{-kr\sin\vartheta}}{re^{i\vartheta}}. \tag{4.14}$$

The complex rotated outgoing wave goes to zero as r goes to infinity so that it can fit in a cavity (for $\sin\vartheta > 0$). A complex rotated incoming wave goes instead to infinity as r goes to infinity. Note that when we expand $P(re^{i\vartheta})$ in B splines it is the coefficients that become complex not the B splines. It is also important to remember that the complex numbers introduced through complex rotation should not be complex conjugated when the Hermitian conjugate of a wavefunction is required in a scalar product.

4.2 Two Electrons

In paper I, II, and IV we diagonalize the two-electron Hamiltonian. The non-relativistic Hamiltonian for two electrons in a potential from a point nucleus is:

$$H = \frac{\mathbf{p}_1^2}{2\mu} + \frac{\mathbf{p}_2^2}{2\mu} + \frac{\mathbf{p}_1 \cdot \mathbf{p}_2}{M} - \frac{Ze^2}{4\pi\epsilon_0 r_1} - \frac{Ze^2}{4\pi\epsilon_0 r_2} + \frac{e^2}{4\pi\epsilon_0 r_{12}}, \tag{4.15}$$

where M is the mass of the nucleus, m is the mass of the electron and $\mu = mM/(m+M)$ is the reduced mass of the electron, Ze is the charge of the nucleus, and $-e$ is the charge of the electron. The mass polarization is small due to the large mass of the nucleus and will be ignored in most calculations. As has been mentioned to solve the Schrödinger equation we diagonalize the Hamiltonian using coupled eigenfunctions of the one-electron Hamiltonian:

$$\langle \{n_a l_a n_b l_b\}\ SL^\pi | H | \{n_c l_c n_d l_d\}\ SL^\pi \rangle. \tag{4.16}$$

The {}-brackets denote that we use anti-symmetrized states. To calculate the matrix elements we need to express the anti-symmetric states as a sum of non-symmetrized states:

$$|\{n_a l_a n_b l_b\} L^\pi M\rangle = \frac{1}{\sqrt{2}} \left(|(n_a l_a)_1 (n_b l_b)_2 L^\pi M\rangle + \pi(-1)^{L+S} |(n_b l_b)_1 (n_a l_a)_2 L^\pi M\rangle \right), \tag{4.17}$$

if $l_a \neq l_b$ or $n_a \neq n_b$, and:

$$|\{nlnl\} L^\pi M\rangle = \begin{cases} |nlnl L^\pi M\rangle \text{ if } (-1)^L = (-1)^S \\ 0 \text{ otherwise} \end{cases} \tag{4.18}$$

if the electrons are equivalent. The only non-diagonal elements in our matrix are due to the $1/r_{12}$ term. Evaluation of the matrix elements for this operator will be done analytically for the angular part and numerically for the radial part. $1/r_{12}$ can be written, e.g. see [34]:

$$\frac{1}{r_{12}} = 4\pi \sum_k \sum_q \frac{1}{2k+1} \frac{r_<^k}{r_>^{k+1}} Y_q^k(\theta_1, \phi_1) Y_q^{*k}(\theta_2, \phi_2), \tag{4.19}$$

where $r_>$ and $r_<$ is the greater and lesser of r_1 and r_2, respectively. Substituting this for $1/r_{12}$ the matrix element can be written [43]:

$$\begin{aligned}
&\langle (n_a l_a)_1 (n_b l_b)_2 \; SL^\pi | \frac{1}{r_{12}} | (n_c l_c)_1 (n_d l_d)_2 \; SL^\pi \rangle \\
&= \sum_k R^k(ab,cd)(-1)^{l_c+l_b+L} \left\{ \begin{array}{ccc} l_a & l_b & L \\ l_d & l_c & k \end{array} \right\} \langle l_a || \overline{C}^k || l_c \rangle \langle l_b || \overline{C}^k || l_d \rangle
\end{aligned} \tag{4.20}$$

$$R^k(ab,cd) = \int\int P_a(r_1) P_b(r_2) \frac{r_<^k}{r_>^{k+1}} P_c(r_1) P_d(r_2) dr_1 dr_2 \tag{4.21}$$

$$\langle l || \overline{C}^k || l' \rangle = (-1)^l [(2l+1)(2l'+1)]^{1/2} \left(\begin{array}{ccc} l & k & l' \\ 0 & 0 & 0 \end{array} \right) \tag{4.22}$$

The $\{\}$ symbol is a 6-j symbol and the $()$ symbol is a 3-j symbol both defined in appendix A. $\langle l || \overline{C}^k || l' \rangle$ is the reduced matrix element of the C tensor [43]. The C tensor is proportional to the spherical harmonics:

$$C_q^k = \sqrt{\frac{4\pi}{2k+1}} Y_q^k(\theta, \phi). \tag{4.23}$$

The only thing left to consider are the radial integrals, which are done numerically either with a discretized grid (Section 4.1.1) or with B splines (Section 4.1.2). With B splines the integration can be done straightforwardly to machine accuracy using Gaussian quadrature. When using a discretized grid care has to be taken not to introduce an unnecessary error at the cusp of $\frac{r_<^k}{r_>^{k+1}}$ at $r_< = r_>$. This can be done by giving the points close to the cusp different weights. The details can be found in Ref. [64].

4.2.1 DESB Quantum Numbers

In our calculations we get the resonant eigenfunction expressed as a sum of coupled eigenstates of the one-electron Hamiltonian. In paper I and paper II we change basis to the DESB basis as described in Section 3.2. To translate from our basis to the DESB basis we use [9]:

$N = n$:

$$\begin{aligned}
&|\{nn\} KT, L^\pi M\rangle \\
&= \sum_{\substack{(l_1 \le l_2)\pi \\ (-1)^{N+l_1+l_2+S} = (-1)^{K+1}}} |\{n l_1 n l_2\} LM\rangle \times D^{KTL}_{n l_1 n l_2} \times \left\{ \begin{array}{ll} \sqrt{2} & \text{if } l_1 \neq l_2 \\ 1 & \text{otherwise} \end{array} \right.
\end{aligned} \tag{4.24}$$

$N \neq n$:

$$|\{Nn\}KT, L^\pi M\rangle = \sum_{(l_1,l_2)\pi} |\{Nl_1nl_2\}LM\rangle \times D^{KTL}_{Nl_1nl_2} \tag{4.25}$$

The sum is a double sum and goes over all l-values with the correct parity. For states where both electrons have the same n-values the l-values must also fulfill the equality under the summation. D is defined by:

$$\begin{aligned} D^{KTL}_{Nl_1nl_2} &= (-1)^{l_2+n-1}\sqrt{(2l_1+1)(2l_2+1)(2J_A+1)(2J_B+1)} \\ &\times \left\{ \begin{array}{ccc} \frac{N-1}{2} & \frac{n-1}{2} & J_A \\ \frac{N-1}{2} & \frac{n-1}{2} & J_B \\ l_1 & l_2 & L \end{array} \right\} \times \left\{ \begin{array}{cc} \sqrt{2} & \text{if } J_A \neq J_B \\ 1 & \text{otherwise} \end{array} \right. \\ J_A &= (K+n+T-1)/2,\ J_B = (K+n-T-1)/2 \end{aligned} \tag{4.26}$$

The $\{\}$ symbol is a 9-j symbol and is defined in appendix A. This transformation rule can also be found in Ref [32, 69]. Possible values for T are:

$$T = 0, 1, ..., \min(L, N-1), \tag{4.27}$$

and for each value of T:

$$K = -(N-T-1), -(N-T-1)+2, ..., N-T-1. \tag{4.28}$$

4.2.2 Relativistic Effects

All the calculations in this thesis are done non-relativistically with one exception, which is in paper I, where we want to investigate the resonances converging to the H($n = 2$) threshold in H^-. It is not the relativistic effects in themselves that are important in this case, but the splitting of the degenerate threshold. Due to relativistic and radiative effects, the threshold splits up into $2s_{1/2}$, $2p_{1/2}$, and $2p_{3/2}$ (the thresholds are to be read nl_j, where j is the orbital and spin angular momenta coupled together). When the resonances that classically converge exponentially towards the threshold (see Section 3.1) come close enough to the threshold (i.e. at a distance comparable to the splitting) the splitting becomes important although it is very small. In principle we will make a non-relativistic calculation with some relativistic corrections that are accurate enough to give

us the correct splitting. We will not consider any relativistic two-particle effects. This is quite reasonable as we are interested in the effect on the threshold, that is, when one electron is at an infinite distance from the nucleus and the two-electron interaction is equal to zero.

Since we know the true threshold energies, H($2s_{1/2}$), H($2p_{1/2}$), and H($2p_{3/2}$), we have first changed the normal non-relativistic calculation in order to be able to use this knowledge. For $2s_{1/2}$ it is straightforward to use the known result for the matrix element $\langle 2s_{1/2}|h_i|2s_{1/2}\rangle$ including relativistic and radiative effects. For $2p_j$ the situation is, due to the existence of two $2p_j$ thresholds, slightly more complicated; For every non-relativistic $|2pn\ell\,{}^1P\rangle$ basis function we will now work with up to three $|2p_jn\ell_{j'}, J=1\rangle$ basis functions. We couple to total $J=1$ since we are interested in photoabsorption from the ground state ($J=0$). Instead of $|2pns\,{}^1P\rangle$ we will thus include $|2p_{1/2}ns_{1/2}, J=1\rangle$ and $|2p_{3/2}ns_{1/2}, J=1\rangle$; and instead of $|2pnd\,{}^1P\rangle$ we will include $|2p_{1/2}nd_{3/2}, J=1\rangle$, $|2p_{3/2}nd_{3/2}, J=1\rangle$, and $|2p_{3/2}nd_{5/2}, J=1\rangle$. As for $2s_{1/2}$ it is now possible to use the known result for the matrix elements $\langle 2p_j|h_i|2p_j\rangle$ including relativistic and radiative effects. The jj-coupled basis functions are in principle linear combinations of several LS-coupled basis functions and this has to be accounted for when the matrix elements of $1/r_{12}$ are calculated. To calculate $1/r_{12}$ for matrix elements where the left, right, or both sides consist of jj-coupled states we just expand them in LS-coupled states, for example:

$$\begin{aligned}
&\langle 3p4d\,{}^1P_{(J=1)}|\frac{1}{r_{12}}|2p_{1/2}3s_{1/2}, J=1\rangle = \\
&\langle 3p4d\,{}^1P_{(J=1)}|\frac{1}{r_{12}}\left(\sqrt{\frac{1}{3}}|2p3s\,{}^1P_{(J=1)}\rangle + \sqrt{\frac{2}{3}}|2p3s\,{}^3P_{(J=1)}\rangle\right) = \\
&\sqrt{\frac{1}{3}}\langle 3p4d\,{}^1P_{(J=1)}|\frac{1}{r_{12}}|2p3s\,{}^1P_{(J=1)}\rangle. \qquad (4.29)
\end{aligned}$$

Basis functions not including $2p_j$ are all LS-coupled (to ${}^1P$). With this scheme we produce the correct splitting of the H($n=2$) threshold, which in fact is enough for our purpose to investigate the effect of the splitting on the series converging to the threshold. The spin-orbit interaction, that causes the $2p_{1/2}-2p_{3/2}$ energy difference, will induce a mixture of ${}^1P^o_{J=1}$, ${}^3P^o_{J=1}$, and ${}^3D^o_{J=1}$ character in the eigenstates of the Hamiltonian. The extent of this mixing is decided through the diagonalization. A noticeable mixing is expected only for states at a distance from threshold comparable to the $2p_{1/2}-2p_{3/2}$ energy difference, i.e. at the same distance where effects on the series itself are expected. This was also found in paper I.

As a last step we have also corrected other basis functions for relativistic effects. We have then used the three relativistic corrections to the non-relativistic one-particle Hamiltonian;

the spin-orbit term, the Darwin term and the $\mathbf{p}^4$ term:

$$\frac{e^2}{8\pi\epsilon_0}\frac{1}{m^2c^2r^3}\mathbf{s}_i\cdot\mathbf{l}_i, \quad \frac{e^2\hbar^2}{8m^2c^2}\delta^3(\mathbf{x}), \quad -\frac{\mathbf{p}^4}{8m^3c^2}. \tag{4.30}$$

The spin-orbit operator is only considered between the jj-coupled states mentioned above. Note that the matrix element of this operator between two ^1P states is identically zero. The two other operators are scalar in orbital space and are taken between all states. This last step gave, however, only minor differences compared to the scheme when only the relativistic effects on the H($n = 2$) thresholds were considered.

4.2.3 Complex Rotation

It is actually only when you have two or more electrons that complex rotation becomes interesting. When we let $r_i \to r_i e^{i\vartheta}$ for each electron, the continuum that starts at each threshold will be rotated 2ϑ just as it was in the one-electron case. Any bound state will be un-affected also just like in the one electron case. What is different is that if the continuum is rotated far enough it might reveal complex eigenvalues that correspond to the poles of the S-matrix. That is they correspond to resonant states. The real part corresponds to the position of the resonance and the imaginary part corresponds to the half width, just like for the model potential in Chapter 2. These points are illustrated schematically in Figure 4.1 showing the eigenvalues of a two-electron atom labeled in the independent particle model. Each eigenvalue is shown as a point in the complex plane. First comes the ground state and the singly excited states on the real axis. Then comes the first threshold with the continuum states rotated 2ϑ. Each eigenstate here represents a state with one electron in the $1s$ state and one free electron with kinetic energy equal to the distance on the real axis between the state and the threshold. Above this the first threshold we find the first resonances. These resonances correspond to doubly excited states represented by complex eigenvalues. Above the resonances comes the second continuum and so on. The eigenvalue of a resonance should theoretically be independent of complex rotation angle, if the angle is large enough to reveal it. Numerically this is never completely true. The limited basis set introduces a small angular dependence. The best eigenvalue is then obtained where the calculated eigenvalue is stationary with respect to ϑ, see Refs. [33, 19].

To calculate photoabsorption the continuum has to be represented in some well defined way. When we use the complex rotation method we get a well defined continuum and to calculate the photoabsorption, for example from the ground state to the continuum, is straightforward. We just sum over all eigenstates of our complex rotated Hamiltonian, both resonant states and continuum states. Rescigno and McKoy discuss this problem in

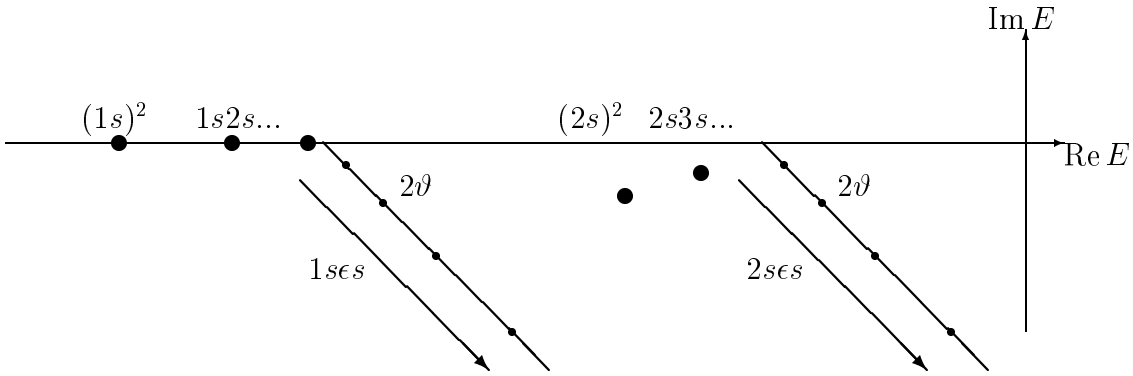

Figure 4.1: A schematic complex rotated spectrum of a two-electron system. States labeled in the independent particle approximation (only s-electrons). Each point represents one eigenvalue. The large points denote stable or resonant states and the small points continuum states.

Ref. [57]. Following them the cross section can be written:

$$\sigma(\omega) = \frac{e^2}{4\pi\epsilon_0}\frac{4\pi}{3}\frac{\omega}{c}\mathrm{Im}\left(\sum_n \frac{\langle\Psi_0|\sum_j r_j e^{i\vartheta}|\Psi_n\rangle\langle\Psi_n|\sum_j r_j e^{i\vartheta}|\Psi_0\rangle}{E_n - E_0 - \hbar\omega}\right), \tag{4.31}$$

where the sum over n goes over all eigenstates of the complete complex Hamiltonian and the sums over j are to be taken over all electrons.

4.3 Three Electrons

The difference between the treatment of the two- and the three-electron system is mainly in the size of the problem, and this is the challenge. To treat three electrons fully is at the limit of what today's computers can handle. It was when we wanted to calculate these systems that we were forced to optimize the knot sequence used to define the B spline as discussed in Section 4.1.2. The three-electron Hamiltonian is diagonalized in paper III, in paper V, and in Section 5.3. The non-relativistic Hamiltonian for three electrons is:

$$\begin{aligned} H &= \frac{\mathbf{p}_1^2}{2\mu} + \frac{\mathbf{p}_2^2}{2\mu} + \frac{\mathbf{p}_3^2}{2\mu} + \frac{1}{M}\left(\mathbf{p}_1\cdot\mathbf{p}_2 + \mathbf{p}_2\cdot\mathbf{p}_3 + \mathbf{p}_3\cdot\mathbf{p}_1\right) \\ &- \frac{Ze^2}{4\pi\epsilon_0}\left(\frac{1}{r_1} + \frac{1}{r_2} + \frac{1}{r_3}\right) + \frac{e^2}{4\pi\epsilon_0}\left(\frac{1}{r_{12}} + \frac{1}{r_{23}} + \frac{1}{r_{31}}\right). \end{aligned} \tag{4.32}$$

The mass polarization terms are, as earlier, neglected on account of being small. We now want to calculate the matrix element between coupled eigenstates of the one-electron Hamiltonian:

$$\langle(\{(n_a l_a n_b l_b)S'L'n_c l_c\})SL^\pi|H|(\{(n_d l_d n_e l_e)S''L''n_f l_f\})SL^\pi\rangle. \tag{4.33}$$

The $\{\}$ are again used to denote that the states are anti-symmetric. A new complication here is that we have to couple to an intermediate angular momentum, L', and an intermediate spin, S', which are non-diagonal in the Hamiltonian. Also the same values of n and l may couple to different intermediate L' and S' for the same total L and S. With three electrons it is no longer possible to symmetrize (and anti-symmetrize) the space and the spin parts separately. It is especially complicated for states with three equivalent electrons. If we couple electron one and two to intermediate S' and L' these must fulfill $(-1)^{S'} = (-1)^{L'}$ to ensure that the state is anti-symmetric. But this state can be expanded in states where we couple electron two and three to intermediate S'' and L'':

$$\begin{aligned}|((nlnl)S'L'nl)SL^\pi\rangle &= \sum_{S''L''}|(nl(nlnl)S''L'')SL^\pi\rangle \\ \times\langle(s(ss)S'')S|((ss)S's)S\rangle&\langle(((l(ll)L'')L|((ll)L'l)L\rangle.\end{aligned} \tag{4.34}$$

In general this sum will contain S'' and L'' that do not fulfill $(-1)^{S''} = (-1)^{L''}$. This means that our state is not anti-symmetric and therefore not physical. What we need to do is to sum over all allowed intermediate L' and S' so that our state becomes anti-symmetric:

$$|nl^3SL\rangle = \sum_{S'L'}|((nlnl)S'L'nl)SL^\pi\rangle c(S',L') \tag{4.35}$$

where the coefficients fulfill:

$$\sum_{S'L'} c(S',L')\langle(s(ss)S'')S|((ss)S's)S\rangle\langle(((l(ll)L'')L|((ll)L'l)L\rangle = 0 \tag{4.36}$$

for $S''+L''$ odd. These coefficients are called coefficients of fractional parentage because there is no one two-particle state to which one extra electron can couple to produce the final state. Fractional parentage is treated in Refs. [43, 55]. As in the two-electron case it is only the inter-electronic interactions we have to worry about. The matrix elements for these operators can be calculated in the same way as in the two-electron case because they are two-electron operators. The details can be found in appendix B.

4.3.1 Complex Rotation

There is one interesting feature in the complex eigenspectra of a three-electron system that does not occur for the two-electron system. Some thresholds are caused by states that are autoionizing states. How does this show up in the eigenspectrum? Let us start by discussing a normal threshold. Here the continuum states lie on a line originating at the threshold rotated an angle 2ϑ from the x-axis (see Figure 4.1), where ϑ is the complex rotation angle. If we would use infinitely many points or infinitely many B splines to describe the radial coordinate the eigenvalues would lie infinitely close on this line starting at the x-axis. Now we have a limited number of points or B splines and therefore we only get a limited number of points with some distance between each. The first eigenvalue is situated close to the x-axis but not exactly on it. This means that there is no continuum state that represents the system minus one electron and one free electron with zero kinetic energy. To understand the situation for a threshold made up of a state which autoionizes we will use an example from paper V. We will look at the He($2s2p\,^3P^o$) threshold in He (see Figure 4.2) for $^4S^e$ even symmetry. The ($2s2p\,^3P^o$) state of helium is auto-ionizing and has a width $\Gamma = 2.99 \times 10^{-4}$a.u. [44]. This corresponds to a negative imaginary part equal to the half width. This means that the continuum states would have started below this value instead of directly below the x-axis if we had used infinitely many basis functions. We use only a limited basis, so we have only a limited number of continuum states, and they will start somewhere below the half width. This can be seen in Figure 4.2. The eigenvalues from one calculation are drawn with circles and the half width is indicated with a line. Next to the circles are some crosses. These are from a calculation using the same parameters, but now excluding all basis functions that contain $1s$ one-electron eigenfunctions. In this calculation the He($2s2p\,^3P^o$) state has no decay channel and the eigenstates come much closer to the threshold. This effect has also been mentioned in Ref. [6].

We would here also like to mention how the threshold position can be determined from a calculation. In the case of a threshold caused by a stable state it is simple. We just draw a line through the continuum eigenvalues and look at what point it crosses the x-axis. This point would correspond to the system minus one electron, and one free electron with zero kinetic energy. In the case of an auto-decaying threshold we instead look where the line reaches the value of the half width of the state that makes up the threshold. It can be seen in the example in Figure 4.2 that this gives a good value compared with another calculation [44]. If we instead would use the intersection with the x-axis the result would be less accurate.

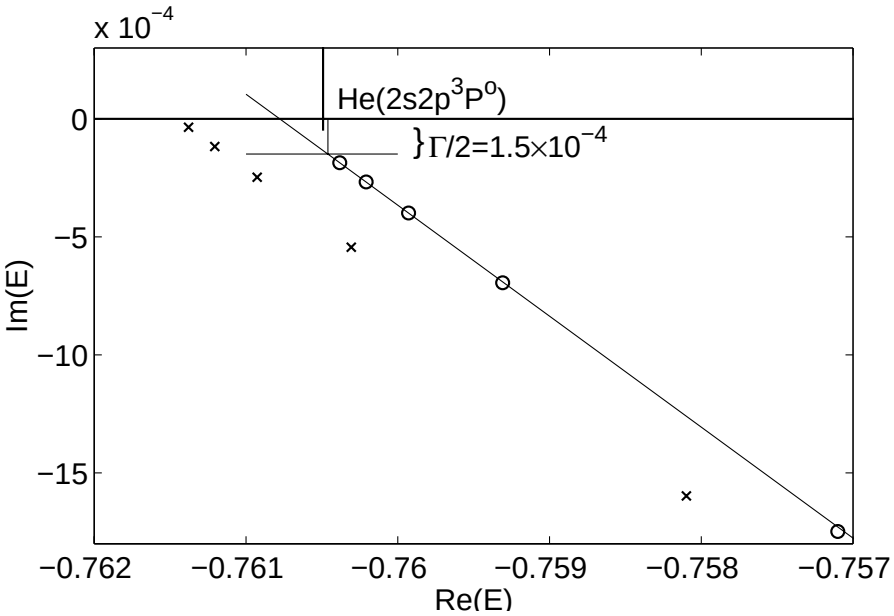

Figure 4.2: Continuum eigenstates of ${}^4S^e$ symmetry close to the He($2s2p\,{}^3P^o$) threshold in He^- from two different runs in paper V. The "o" eigenstates are from a complete diagonalization of the Hamiltonian and the "x" are from a diagonalization where all basis functions that consist of at least one $1s$ one-electron function are excluded. The straight line is the position for this threshold as published in Ref. [44]. All units are in atomic units for infinite heavy nucleus.

Chapter 5

Some Results

It is not the purpose of this chapter to recapture the results presented in the different papers. The purpose is instead to present some new results, and to compare the results of our papers with results which were not available when the papers were written. In the first two sections the results of paper I and paper III are compared with some new results. In the last section we present some results for H^{2-} that have not been published before.

5.1 H^- Resonances Converging to the H$(n = 2)$ Threshold

As was mentioned in Section 3.1, in H^- we expect an infinite series of resonances converging exponentially to all thresholds, because the thresholds are degenerate. The thresholds are, however, actually not completely degenerate. When relativistic and radiative effects are considered the thresholds split up according to orbital angular momentum l and total spin j. For $n = 2$ we get three thresholds corresponding to H$(2s_{1/2})$, H$(2p_{1/2})$, and H$(2p_{3/2})$. This splitting is very small as is usually the case for low Z, but as the resonances come closer and closer to the threshold it becomes important. This means that we get relativistic effects also for the least relativistic of all systems, the $Z = 1$ system. Without the degeneracy the outer electron would experience an induced dipole proportional to $1/r^4$, instead of the $1/r^2$ potential for degenerate thresholds.This means that as the non-degeneracy becomes important we can expect the outer electron to experience a weaker potential. It is reasonable to expect that this effect will first produce deviations from Equation (3.3) and then finally the termination of the series. This does not mean that there cannot be resonances above the different thresholds, but only that we can expect the exponentially converging series to come to an end.

Table 5.1: Relativistic results for all $^1P^o$ resonances of H^- below the $H(2p_{1/2})$ threshold at -0.125002082 a.u. Energies are relative to complete breakup and atomic units are used. Our results are for infinitely heavy nucleus.

Paper I		Purr and Friedrich[a]	Chen[b]	
E	Γ	E	E	Γ
-0.1260509	1.37×10^{-6}	-0.1260505	-0.1260511	1.31×10^{-6}
-0.1250365	7×10^{-8}	-0.12503645	-0.1250364	7.0×10^{-8}
-0.1250028	2×10^{-9}	-0.12500279	-0.12500281	2.6×10^{-9}

[a] Reference [54]

[b] Reference [14]

To investigate these effects we did a semi-relativistic calculation also including some radiative effects. More details about the calculation can be found in paper I and also in Section 4.2.2. The main idea was to get the thresholds correct as it is the splitting rather than the relativistic effects themselves that affect the resonances. In the relativistic calculation already the third resonance is clearly affected and the fourth resonance disappears. In Table 5.1 our results are compared with two later calculations also taking into account the relativistic splitting. Purr and Friedrich use a semiempirical coupled-channel calculation [54]. To fix four parameters they used our results for the two lowest resonances of $^1P^o$ symmetry and the results of Ref. [13] for the two lowest resonances of $^3P^o$ symmetry. This means that the agreement for the first two resonances are of no importance. Chen [14] uses a saddle-point complex rotation method with B splines to calculate all resonances *ab initio*. Both of these calculations agree with our conclusion that the series is terminated after the third resonance. Bylicki and Nicolaides [12] calculate the resonances non-relativistically and argue that the fourth resonance may be situated above the $H(2p_{1/2})$ threshold rather unaffected by the splitting, or possibly transformed into a relativistic shape resonance. We hold the first alternative to be extremely unlikely as we would have seen it in our relativistic calculation. The second alternative is maybe possible. There could be some reasons why we do not see it in our calculation, for example if it is extremely extended. However even if this is true we do not think that this contradicts the fact that the series of resonances converging to the threshold is terminated, as this shape resonance would not belong to this exponentially converging series.

5.2 $^4S^e$ Resonances of He^- Below the $He^+(n = 1)$ Threshold

When the development of the three-electron program was close to completion, we needed to find a system which would be suitable for the program and for which there were results

to compare with. Doubly excited states of $^4S^e$ symmetry in He^- turned out to be excellent as a test case. These states involve three open shells so that a three-electron program would be useful, but the inner electron is pretty well described as a $1s$ electron, so that small test runs, where the inner electron is kept in $1s$, could be made. It existed one resonance that had been both measured [39, 40] and calculated [82]. Furthermore the same group that had done the two measurements of the resonance were performing new measurements to try to find more resonances. The new experiment [38] found twelve previously unobserved resonances, and two of these could be identified as $^4S^e$ with the help of our calculation. The agreement between our results and the experiment is in general good. For the width of the lowest resonance there is a small disagreement. It is therefore interesting to note that there are now two more calculations [56, 46] that also find a smaller width than the experiment. All available results for the four resonances are presented in Table 5.2.

5.3 Resonant States in H^{2-}

When the three-electron project was started it was with one particular goal in mind. That was to see if there was any resonances in H^{2-}. Such a system seemed to be an excellent task for the program. The three-electron correlation in a resonant state in H^{2-} if such a state existed must be great. There was an old controversy about the existence of resonances in H^{2-} which was more or less settled. In the early seventies Walton, Peart, and Dolder [76, 77, 53] had found two resonances in the H production when electrons were collided with H^-. These resonances were attributed to the formation of auto-detaching states of H^{2-}. Taylor and Thomas [72, 73] performed calculations and found also two resonances in H^{2-}, which roughly agreed with the experiment. Later calculations did however not find the resonances or reached ambiguous results (references can be found in Ref. [58]). Robicheaux, Wood, and Greene [58] calculated the effect of the resonances found in Ref. [72, 73] on the H production and found that they could not explain the features obtained in the experiments. The conclusion was that the calculated resonances were spurious states and the result of neglecting important decay channels. An improved experiment was set up by Andersen *et al.* [3]. Instead of H they used D but this should have no effect on the electronic properties. They also found no evidence for any resonances. There could however still exist resonances that were for different reasons not visible in the experiment. To find such resonances was the aim of our project when it started. Unfortunately, two other calculations found new resonances in H^{2-} before we did. The first to find a resonance was Sommerfeld *et al.* [70, 71] in 1996. Bylicki and Nicolaides [11] in 1998 confirmed the resonance with good agreement and also found one more resonance. The resonances found are of $^4S^o$ symmetry, and this explains why they were not found in the experiment of Ref. [3]. In this experiment electron impact on D^- in its ground state, $^1S^e$, was studied, and the D yield was measured. The probability to go to $^4S^o$ from the

Table 5.2: Comparison of the results of paper III with available experimental and theoretical results.

	E-E($1s2s2p$)^4P(eV)	Γ(meV)
$1s3s4s$		
Paper III	2.95924	0.16
Xi and Froese Fischer[a]		
Length form	2.95907	0.19
Velocity form	2.95908	0.18
Ramsbottom and Bell[b]	2.95983	0.16
Liu and Starace[c]		
Length form	2.959248	0.154
Velocity form	2.959248	0.154
Experiment[d]	2.959255(7)	0.19(3)
Experiment[e]	2.959260(6)	0.20(2)
$1s4s5s$		
Paper III	3.81419	0.73
Liu and Starace[c]	3.814225	0.8
Experiment[f]	3.81429(9)	0.8(2)
$1s4d5d$		
Paper III	3.95158	0.15
Liu and Starace[c]	3.951457	0.2
Experiment[f]	3.9515(1)	0.3(2)
$1s5s6s$		
Paper III	4.18779	5.5
Liu and Starace[c]	4.187816	6.9

[a] Reference [82]
[b] Reference [56]
[c] Reference [46]
[d] Reference [39], partial cross section to $1s2s\,^3S$.
[e] Reference [40], partial cross section to $1s2p\,^3P$.
[f] Reference [38]

ground state is very small as a spin-flip is needed. Furthermore, the resonance is predicted to be mainly in *ppp* so both electrons in D^- need to change orbital angular momentum in the collision. There is still some controversy about these resonances as Morishita, Lin, and Bao [49] claim that no resonances of $^4S^o$ symmetry can exist in H^{2-}. Unfortunately

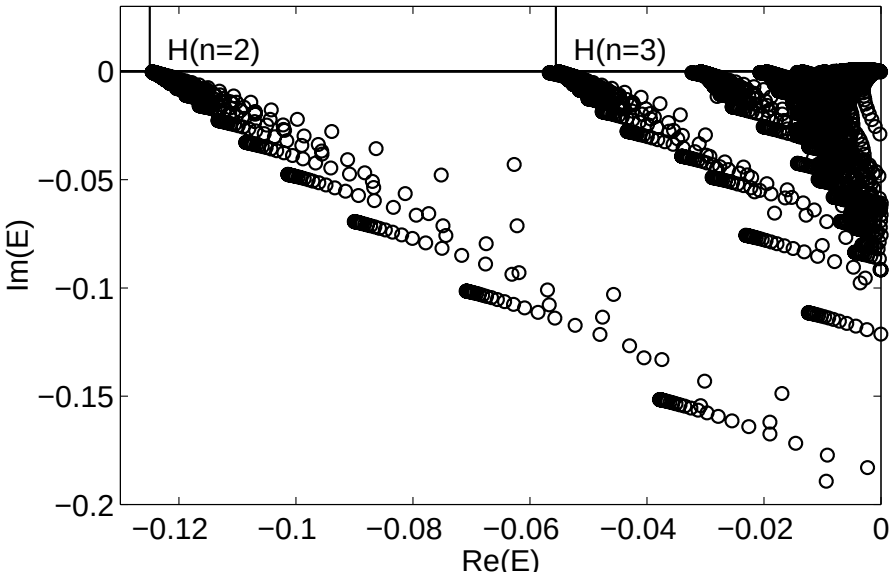

Figure 5.1: All complex eigenvalues to the complex rotated Hamiltonian of H^{2-} for $^4S^o$ symmetry below E= 0 are plotted in the complex plane. Energy is relative to complete break-up of the system and are given in atomic units. The Hamiltonian was complex rotated 30°. The cavity size was 2000 a.u. We used 45 knots and $k = 5$ to create 38 B splines. The knot sequence was linear up to 12 a.u. exponential up to approximately 1686 a.u. and then there where no points until 2000 a.u. The four one electron eigenfunctions with highest energy where not used to create the basis set, so that we had 34 one-electron eigenfunctions. Only the *ppp* angular configuration was used. The resonance eigenvalue can be seen clearly separated from the H($n = 2$) two electron continuum.

our method is so similar to the one used in Ref. [11] that we cannot add much to this controversy. We still like to present the results from one run on H^{2-} for $^4S^o$ symmetry in this thesis. No optimization has been done and we have only considered *ppp* electrons. Parameters were partly chosen with guidance from Ref. [11] and partly chosen by chance. The resonance as can be seen in Figure 5.1 is very clearly visible. Our result for the complex pole, $(-0.063 - i0.043)$a.u. agrees with the result of Ref. [11] when they also use only *ppp* electrons. The full result in their paper was $(-0.0725 - i0.0310)$a.u. Because we also find the resonance the probability for it to be an artefact of the basis set must be very small. What we have found here is of course as always a complex pole in the S matrix and usually we associate these poles with resonances. Is this reasonable in the present case? One way to answer the question is to say that a resonance is a complex pole in the S matrix per definition. A more interesting definition might be to require a resonance to be visible as a local structure in some spectrum, at least in principle. The resonances found here will be very wide, but will probably none the less make some difference to a spectrum. A calculation of, for example, the production of neutral H when H^- in the metastable state $2p^2\ ^3P$ is bombarded by electrons would be very interesting, although

the experiment might be almost impossible to do.

Concluding Remarks

This thesis presents several studies of both doubly and triply excited resonant states. The main contribution of this work is the development of a method that can treat three electrons on equal terms and do it so well that these very correlated systems can be handled. The method has been proven to work in paper III for doubly excited states and finally in paper V for triply excited states in He^-. The exact circumstances have to be considered to decide if relativistic effects need attention in a calculation. In paper I they prove to be important in one of the lightest of atomic systems, H^- . To describe the electron correlation in doubly excited states different new quantum numbers have been suggested by different authors. One such suggestion, the DESB quantum numbers, has been investigated from different aspects in papers I-IV. The general idea is to use our high precision *ab initio* calculations to test how well these quantum numbers really describe doubly excited states. One important contribution is in Paper II, where it is shown that the expectation value of the cosine of the inter-electronic angle can be studied to determine the amount of DESB state mixing. Another important contribution is the identification of a state in Li^- that violates a propensity rule for doubly excited states.

Acknowledgements

I would like to start with expressing my gratitude to all former and present members of the Atomic Physics Group. You have all been part of my experience as a PhD student. Then I would like to continue with some people that have all been very important to my work. Eva Lindroth, my supervisor, has used an enormous amount of time and effort to help me and to work on my projects. She has also always encouraged a true discussion without barriers. Andre Bürgers has been my roommate for most of the time. To him I also owe a lot. We have worked together on some projects, but he has also helped me a lot on my other projects. He is for example the one who taught me Latex. Josef Anton has been crucial to the later part of my work. Without his computer knowledge and willingness to devote his time to adapt the computers to my calculations, many of the results on triply excited He^- might not have been achieved. Also his German beer has been most welcome. I would like to thank Reinhold Schuch for the group seminars that have been interesting and full of discussions. These meetings have also been important as a glue in the group. I would like to thank Dag Hanstorp for sharing his measurements with us and Kieth MacAdam for proofreading this thesis so carefully. Finally I would like to thank Jenny for her support and help with the proofreading.

Appendix A

The 3-j, 6-j, and 9-j Symbols

The definitions of these symbols are taken from ref. [43]. The 3-j symbol is basically a Clebsch-Gordan coefficient multiplied by a factor to make it symmetric between the different angular momenta.

$$\begin{pmatrix} j_1 & j_2 & j_3 \\ m_1 & m_2 & m_3 \end{pmatrix} = (-1)^{j_1-j_2-m_3}(2j_3+1)^{-1/2}\langle j_1 m_1, j_2 m_2 | j_3 m_3\rangle \tag{A.1}$$

The 6-j symbol is in a similar way defined to have a high degree of symmetry. It is related to another recoupling constant.

$$\begin{pmatrix} j_1 & J_{12} & j_2 \\ j_3 & J_{23} & J \end{pmatrix} =$$
$$(-1)^{j_1+j_2+j_3+J}(2J_{12}+1)^{-1/2}(2J_{23}+1)^{-1/2}\langle (j_1 j_2)J_{12}, j_3, J | j_1, (j_2 j_3)J_{23}, J\rangle \tag{A.2}$$

It can also be written as a sum of products of 3-j symbols:

$$\begin{aligned} \begin{Bmatrix} j_1 & j_2 & j_3 \\ j_4 & j_5 & j_6 \end{Bmatrix} &= \sum_{\text{all } m} (-1)^{j_1-m_1+j_2-m_2+j_3-m_3+j_4-m_4+j_5-m_5+j_6-m_6} \\ &\times \begin{pmatrix} j_1 & j_2 & j_3 \\ -m_1 & -m_2 & -m_3 \end{pmatrix} \begin{pmatrix} j_1 & j_5 & j_6 \\ m_1 & -m_5 & m_6 \end{pmatrix} \\ &\times \begin{pmatrix} j_2 & j_6 & j_4 \\ m_2 & -m_6 & m_4 \end{pmatrix} \begin{pmatrix} j_3 & j_4 & j_5 \\ m_3 & -m_4 & m_5 \end{pmatrix} \end{aligned} \tag{A.3}$$

The 9-j symbol also relates to a recoupling constant:

$$\begin{Bmatrix} s_1 & s_2 & S \\ l_1 & l_2 & L \\ j_1 & j_2 & J \end{Bmatrix} = (2j_1+1)^{-1/2}(2j_2+1)^{-1/2}(2S+1)^{-1/2}(2L+1)^{-1/2} \times \langle (s_1 s_2)S, (l_1 l_2)L, J | (s_1 l_1)j_1, (s_2 l_2)j_2, J \rangle, \quad \text{(A.4)}$$

and it can also be written as a sum of products of 3-j symbols:

$$\begin{Bmatrix} j_{11} & j_{12} & j_{13} \\ j_{21} & j_{22} & j_{23} \\ j_{31} & j_{32} & j_{33} \end{Bmatrix} = \sum_{\text{all } m} \begin{pmatrix} j_{11} & j_{12} & j_{13} \\ m_{11} & m_{12} & m_{13} \end{pmatrix} \begin{pmatrix} j_{21} & j_{22} & j_{23} \\ m_{21} & m_{22} & m_{23} \end{pmatrix} \begin{pmatrix} j_{31} & j_{32} & j_{33} \\ m_{31} & m_{32} & m_{33} \end{pmatrix} \times \begin{pmatrix} j_{11} & j_{21} & j_{31} \\ m_{11} & m_{21} & m_{31} \end{pmatrix} \begin{pmatrix} j_{12} & j_{22} & j_{32} \\ m_{12} & m_{22} & m_{32} \end{pmatrix} \begin{pmatrix} j_{13} & j_{23} & j_{33} \\ m_{13} & m_{23} & m_{33} \end{pmatrix}. \quad \text{(A.5)}$$

Appendix B

The Matrix Elements of the Three-electron Hamiltonian

Here we will give the details of the calculation of the matrix elements of the three-electron Hamiltonian:

$$\langle(\{(n_a l_a n_b l_b)S'L'n_c l_c\})SL^\pi|H|(\{(n_d l_d n_e l_e)S''L''n_f l_f\})SL^\pi\rangle. \tag{B.1}$$

The only non-diagonal parts of the Hamiltonian is the electron-electron interaction operators. In principle there is no difference to calculate these for the three-electron Hamiltonian compared to the two-electron Hamiltonian (4.20). For future reference we will still give the exact form for all operator and symmetry combinations. To describe the different kets in the anti-symmetrization of the basis kets we will introduce the following notation. If we discuss a state ket, $|((n_a l_a n_b l_b)S'L'n_c l_c)SL^\pi\rangle$, $|3\ 2\ 1\rangle$ will mean that it is particle three which has quantum numbers n_a and l_a, particle two which has quantum numbers n_b and l_b, and particle one which has quantum numbers n_c and l_c. No matter which particle has which set of quantum numbers we will always couple l_a and l_b to the intermediate L', and s_a and s_b to the intermediate S'. In this notation an anti-symmetric state ket can be written:

$$\begin{aligned}|(\{(n_a l_a n_b l_b)S'L'n_c l_c\})SL^\pi\rangle \;&=\; \frac{1}{\sqrt{6}}\left(|1\ 2\ 3\rangle - |2\ 1\ 3\rangle + |2\ 3\ 1\rangle\right.\\ &\quad\left. - |3\ 2\ 1\rangle + |3\ 1\ 2\rangle - |1\ 3\ 2\rangle\right).\end{aligned} \tag{B.2}$$

The different matrix elements that we need to calculate follow.

$$\begin{aligned}\langle 1\ 2\ 3|r_{12}^{-1}|1\ 2\ 3\rangle &= \sum_k R^k(ab,de)\langle l_a||\overline{C}^k||l_d\rangle\langle l_b||\overline{C}^k||l_e\rangle \\ &\times \delta(S',S'')\delta(l_c,l_f)\delta(L',L'')(-1)^{l_b+l_d+L'}\left\{\begin{array}{ccc} l_a & l_b & L' \\ l_e & l_d & k \end{array}\right\} \end{aligned} \tag{B.3}$$

$$\begin{aligned}\langle 1\ 2\ 3|r_{23}^{-1}|1\ 2\ 3\rangle &= \sum_k R^k(bc,ef)\langle l_b||\overline{C}^k||l_e\rangle\langle l_c||\overline{C}^k||l_f\rangle \\ &\times \delta(S',S'')\delta(l_a,l_d)(-1)^{l_a+l_e+l_c+L'+L''+L+k}\sqrt{(2L'+1)(2L''+1)} \\ &\times \left\{\begin{array}{ccc} L' & l_c & L \\ l_f & L'' & k \end{array}\right\}\left\{\begin{array}{ccc} l_b & L' & l_a \\ L'' & l_e & k \end{array}\right\} \end{aligned} \tag{B.4}$$

$$\begin{aligned}\langle 1\ 2\ 3|r_{31}^{-1}|1\ 2\ 3\rangle &= \sum_k R^k(ca,fd)\langle l_c||\overline{C}^k||l_f\rangle\langle l_a||\overline{C}^k||l_d\rangle \\ &\times \delta(S',S'')\delta(l_b,l_e)(-1)^{l_a+l_b+l_c+L+k}\sqrt{(2L'+1)(2L''+1)} \\ &\times \left\{\begin{array}{ccc} L' & l_c & L \\ l_f & L'' & k \end{array}\right\}\left\{\begin{array}{ccc} l_a & L' & l_b \\ L'' & l_d & k \end{array}\right\} \end{aligned} \tag{B.5}$$

To get the results for $\langle 1\ 2\ 3|r_{xx'}^{-1}|2\ 1\ 3\rangle$ replace d with e and vice versa and multiply with $(-1)^{l_d+l_e+L''+1+S''}$.

$$\begin{aligned}\langle 1\ 2\ 3|r_{12}^{-1}|2\ 3\ 1\rangle &= \sum_k R^k(ab,fd)\langle l_a||\overline{C}^k||l_f\rangle\langle l_b||\overline{C}^k||l_d\rangle \\ &\times (-1)^{2S+S''-1}\sqrt{(2S'+1)(2S''+1)}\left\{\begin{array}{ccc} s & S' & s \\ s & S'' & S \end{array}\right\} \\ &\times \delta(l_c,l_e)(-1)^{l_b+l_c+l_d+l_f+L'+L''}\sqrt{(2L'+1)(2L''+1)} \\ &\times \left\{\begin{array}{ccc} l_d & l_f & L' \\ l_a & l_b & k \end{array}\right\}\left\{\begin{array}{ccc} L' & l_c & L \\ L'' & l_f & l_d \end{array}\right\} \end{aligned} \tag{B.6}$$

$$
\begin{aligned}
\langle 1\ 2\ 3|r_{23}^{-1}|2\ 3\ 1\rangle &= \sum_k R^k(bc,de)\langle l_b||\overline{C}^k||l_d\rangle\langle l_c||\overline{C}^k||l_e\rangle \\
&\times (-1)^{2S+S''-1}\sqrt{(2S'+1)(2S''+1)}\left\{\begin{array}{ccc} s & S' & s \\ s & S'' & S \end{array}\right\} \\
&\times \delta(l_a,l_f)(-1)^{l_b+l_d}\sqrt{(2L'+1)(2L''+1)} \\
&\times \left\{\begin{array}{ccc} l_c & L'' & l_b \\ l_d & k & l_e \end{array}\right\}\left\{\begin{array}{ccc} L' & l_c & L \\ L'' & l_a & l_b \end{array}\right\} \qquad \text{(B.7)}
\end{aligned}
$$

$$
\begin{aligned}
\langle 1\ 2\ 3|r_{31}^{-1}|2\ 3\ 1\rangle &= \sum_k R^k(ca,ef)\langle l_c||\overline{C}^k||l_e\rangle\langle l_a||\overline{C}^k||l_f\rangle \\
&\times (-1)^{2S+S''-1}\sqrt{(2S'+1)(2S''+1)}\left\{\begin{array}{ccc} s & S' & s \\ s & S'' & S \end{array}\right\} \\
&\times \delta(l_b,l_d)(-1)^{L'+l_b+l_f}\sqrt{(2L'+1)(2L''+1)} \\
&\times \left\{\begin{array}{ccc} L' & l_c & L \\ l_b & l_e & L'' \\ l_a & k & l_f \end{array}\right\} \qquad \text{(B.8)}
\end{aligned}
$$

To get the results for $\langle 1\ 2\ 3|r_{xx'}^{-1}|3\ 2\ 1\rangle$ again replace d with e and vice versa and multiply with $(-1)^{l_d+l_e+L''+1+S''}$.

$$
\begin{aligned}
\langle 1\ 2\ 3|r_{12}^{-1}|3\ 1\ 2\rangle &= \sum_k R^k(ab,ef)\langle l_a||\overline{C}^k||l_e\rangle\langle l_b||\overline{C}^k||l_f\rangle \\
&\times (-1)^{S'}\sqrt{(2S'+1)(2S''+1)}\left\{\begin{array}{ccc} S' & s & S \\ S'' & s & s \end{array}\right\} \\
&\times \delta(l_c,l_d)(-1)^{k}\sqrt{(2L'+1)(2L''+1)} \\
&\times \left\{\begin{array}{ccc} L' & l_e & l_f \\ k & l_b & l_a \end{array}\right\}\left\{\begin{array}{ccc} L' & l_c & L \\ L'' & l_f & l_e \end{array}\right\} \qquad \text{(B.9)}
\end{aligned}
$$

$$\begin{aligned}
\langle 1\ 2\ 3|r_{23}^{-1}|3\ 1\ 2\rangle &= \sum_k R^k(bc,fd)\langle l_b||\overline{C}^k||l_f\rangle\langle l_c||\overline{C}^k||l_d\rangle \\
&\times (-1)^{S'}\sqrt{(2S'+1)(2S''+1)}\left\{\begin{array}{ccc} S' & s & S \\ S'' & s & s \end{array}\right\} \\
&\times \delta(l_a,l_e)(-1)^{l_d+l_a+L''+k}\sqrt{(2L'+1)(2L''+1)} \\
&\times \left\{\begin{array}{ccc} L' & l_c & L \\ l_a & l_d & L'' \\ l_b & k & l_f \end{array}\right\} \qquad \text{(B.10)}
\end{aligned}$$

$$\begin{aligned}
\langle 1\ 2\ 3|r_{31}^{-1}|3\ 1\ 2\rangle &= \sum_k R^k(ca,de)\langle l_c||\overline{C}^k||l_d\rangle\langle l_a||\overline{C}^k||l_e\rangle \\
&\times (-1)^{S'}\sqrt{(2S'+1)(2S''+1)}\left\{\begin{array}{ccc} S' & s & S \\ S'' & s & s \end{array}\right\} \\
&\times \delta(l_b,l_f)(-1)^{l_a+l_b+l_d+l_e+L'+L''+k}\sqrt{(2L'+1)(2L''+1)} \\
&\times \left\{\begin{array}{ccc} l_c & L'' & l_a \\ e & k & l_d \end{array}\right\}\left\{\begin{array}{ccc} L' & l_c & L \\ L'' & l_b & l_a \end{array}\right\} \qquad \text{(B.11)}
\end{aligned}$$

To get the results for $\langle 1\ 2\ 3|r_{xx'}^{-1}|1\ 3\ 2\rangle$ once again replace d with e and vice versa and multiply with $(-1)^{l_d+l_e+L''+1+S''}$.

Bibliography

[1] For an account of the early contributions to the complex rotation method see the whole No. 4 issue of Int. J. Quantum Chem. **14** (1978).

[2] J. Aguilar and J. M. Combes. *Commun. Math. Phys.*, 22:269, 1971.

[3] L. H. Andersen, D. Mathur, H. T. Schmidt, and L. Vejby-Christensen. *Phys. Rev. Lett.*, 74:892, 1995.

[4] E. P. Auger. *J. Phys. Radium*, 6:205, 1925.

[5] P. Balling, P. Kristiansen, U. V. Pedersen, V. V. Petrunin, L. Præstegaard, H. H. Haugen, and T. Andersen. *Phys. Rev. Lett.*, 77:2905, 1996.

[6] E. Balslev. In S. Albeverio, L. S. Ferreira, and L. Streit, editors, *Resonances - Models and Phenomena*, Berlin, 1984. Springer-Verlag.

[7] E. Balslev and J. M. Combes. *Commun. Math. Phys.*, 22:280, 1971.

[8] H. Z. Beutler. *Z. Physik*, 86:495, 1933.

[9] N. Brandefelt. Master's thesis, Stockholm University, 1996.

[10] S. J. Buckman and C. W. Clark. *Rev. Mod. Phys.*, 66:539, 1994.

[11] M. Bylicki and C. A. Nicolaides. *J. Phys. B*, 31:L685, 1998.

[12] M. Bylicki and C. A. Nicolaides. *Phys. Rev. A*, 61:052508, 2000.

[13] M. K. Chen. *J. Phys. B*, 30:1669, 1997.

[14] M. K. Chen. *J. Phys. B*, 32:L487, 1999.

[15] K. T. Compton and J. C. Boyce. *J. Franklin Inst.*, 205:497, 1928.

[16] J. W. Cooper, U. Fano, and F. Prats. *Phys. Rev. Lett.*, 10:518, 1963.

[17] D. Coster and R. de L. Kronig. *Physica*, 2:13, 1935.

[18] C. deBoor. *A Practical Guide to Splines*. Springer-Verlag, New York, 1978.

[19] G. D. Doolen. *J. Phys. B: Atom. Molec. Phys.*, 8:525, 1975.

[20] U. Fano. *Phys. Rev.*, 124:1866, 1961.

[21] U. Fano and J. W. Cooper. *Phys. Rev.*, 137:A1364, 1965.

[22] J. M. Feagin and J. S. Briggs. *Phys. Rev. Lett.*, 57:984, 1986.

[23] J. M. Feagin and J. S. Briggs. *Phys. Rev. A*, 37:4599, 1986.

[24] M. Gailitis and R. Damburg. *Proc. Phys. Soc.*, 82:192, 1963.

[25] B. C. Gou, Z. Chen, and C. D. Lin. *Phys. Rev. A*, 43:3260, 1991.

[26] P. T. Greenland. *Nature*, 335:298, 1988.

[27] P. G. Harris, H. C. Bryant, A. H. Mohagheghi, R. A. Reeder, H. Sharifian, C. Y. Tang, H. Tootoonchi, J. B. Donahue, C. R. Quick, D. C. Rislove, W. W. Smith, and J. E. Stewart. *Phys. Rev. Lett.*, 65(3):309, 1990.

[28] D. R. Herrick. *Phys. Rev. A*, 12:413, 1975.

[29] D. R. Herrick. *Adv. Chem. Phys.*, 52:1, 1983.

[30] D. R. Herrick and M. E. Kellman. *Phys. Rev. A*, 21:418, 1980.

[31] D. R. Herrick, M. E. Kellman, and R. D. Poliak. *Phys. Rev. A*, 22:1517, 1980.

[32] D. R. Herrick and O. Sinanoğlu. *Phys. Rev. A*, 11:97, 1975.

[33] Y. K. Ho. *Phys. Rep.*, 99:1, 1983.

[34] J. D. Jackson. *Classical Electrodynamics*. John Wiley & Sons, Inc., New York, 2nd edition, 1975.

[35] W. R. Johnson, S. A. Blundell, and J. Sapirstein. *Phys. Rev. A*, 37:307, 1988.

[36] W. R. Johnson and J. Sapirstein. *Phys. Rev. Lett.*, 57:1126, 1986.

[37] M. E. Kellman and D. R. Herrick. *Phys. Rev. A*, 22:1536, 1980.

[38] I. Y. Kiyan, U. Berzinsh, D. Hanstorp, and D. J. Pegg. *Phys. Rev. Lett.*, 81:2874, 1998.

[39] A. E. Klinkmüller, G. Haeffler, D. Hanstorp, I. Y. Kiyan, U. Berzinsh, C. W. Ingram, D. J. Pegg, and J. R. Peterson. *Phys. Rev. A*, 56:2788, 1997.

[40] A. E. Klinkmüller, G. Haeffler, D. H. I. Y. Kiyan, U. Berzinsh, and D. J. Pegg. *J. Phys. B.*, 31:2549, 1998.

[41] C. D. Lin. *Phys. Rev. A*, 29:1019, 1984.

[42] C. D. Lin. *Physica Scripta*, T46:65, 1993.

[43] I. Lindgren and J. Morrison. *Atomic Many-Body Theory.* Series on Atoms and Plasmas. Springer-Verlag, New York Berlin Heidelberg, second edition, 1986.

[44] E. Lindroth. *Phys. Rev. A*, 49:4473, 1994.

[45] E. Lindroth. *Phys. Rev. A*, 52:2737, 1995.

[46] C. N. Liu and A. F. Starace. *Phys. Rev. A*, 60:4647, 1999.

[47] R. P. Madden and K. Codling. *Phys. Rev. Lett.*, 10:516, 1963.

[48] E. Merzbacher. *Quantum Mechanics.* John Wiley & Sons, Inc., New York, 1961.

[49] T. Morishita, C. D. Lin, and C. G. Bao. *Phys. Rev. Lett.*, 80:464, 1998.

[50] C. A. Nicolaides. *Phys. Rev. A*, 6:2078, 1972.

[51] C. A. Nicolaides and D. R. Beck. *Phys. Rev. Lett.*, 38:683, 1977.

[52] C. A. Nicolaides and T. Mercouris. *J. Phys. B*, 29:1151, 1996.

[53] B. Pert and K. T. Dolder. *J. Phys. B*, 6:1497, 1973.

[54] T. Purr and H. Friedrich. *Phys. Rev. A.*, 57:4279, 1998.

[55] G. Racah. *Phys. Rev.*, 63:367, 1943.

[56] C. A. Ramsbottom and K. L. Bell. *J. Phys. B*, 32:1315, 1999.

[57] T. N. Rescigno and V. McKoy. *Phys. Rev. A*, 12:522, 1975.

[58] F. Robicheaux, R. P. Wood, and C. H. Greene. *Phys. Rev. A*, 49:1866, 1994.

[59] J. M. Rost and J. S. Briggs. *J. Phys. B*, 23:L339, 1990.

[60] J. M. Rost and J. S. Briggs. *J. Phys. B*, 24:4293, 1991.

[61] J. M. Rost, J. S. Briggs, and J. M. Feagin. *Phys. Rev. Lett.*, 66:1642, 1991.

[62] J. M. Rost, R. Gersbacher, K. Richterand, J. S. Briggs, and D. Wintgen. *J. Phys. B*, 24:2455, 1991.

[63] H. R. Sadeghpour and C. H. Greene. *Phys. Rev. Lett.*, 65:313, 1990.

[64] S. Salomonson and P. Öster. *Phys. Rev. A*, 40:5559, 1989.

[65] G. J. Schulz. *Rev. Mod. Phys.*, 45:378, 1973.

[66] A. S. Shenstone. *Phys. Rev.*, 38:873, 1931.

[67] B. Simon. *Commun. Math. Phys.*, 27:1, 1972.

[68] B. Simon. *Ann. Math.*, 97:247, 1973.

[69] O. Sinanoğlu and D. R. Herrick. *J. Chem. Phys.*, 62:886, 1975.

[70] T. Sommerfeld, U. V. Riss, H.-D. Meyer, and L. S. Cederbaum. *Phys. Rev. Lett.*, 77:470, 1996.

[71] T. Sommerfeld, U. V. Riss, H.-D. Meyer, and L. S. Cederbaum. *Phys. Rev. A*, 55:1903, 1997.

[72] H. S. Taylor and L. D. Thomas. *Phys. Rev. Lett.*, 28:1091, 1972.

[73] L. D. Thomas. *J. Phys. B*, 7:L97, 1974.

[74] C. J. van Winter. *Math. Anal. Appl.*, 47:633, 1974.

[75] A. Vollweiter, J. M. Rost, and J. S. Briggs. *J. Phys. B*, 24:L155, 1991.

[76] D. S. Walton, B. Pert, and K. T. Dolder. *J. Phys. B*, 3:L148, 1970.

[77] D. S. Walton, B. Pert, and K. T. Dolder. *J. Phys. B*, 4:1343, 1970.

[78] S. Watanabe and C. D. Lin. *Phys. Rev. A*, 34:823, 1986.

[79] R. Widdington and H. Priestley. *Proc. Roy. Soc.*, A145:462, 1934.

[80] S. Wolfram. *The Mathematica Book*. Wolfram Media/Cambridge University Press, New York, 4th edition, 1999.

[81] C. Wulfman and K. Sukeyuki. *J. Chem. Phys.*, 23:367, 1973.

[82] J. Xi and C. Froese-Fischer. *Phys. Rev. A*, 53:3169, 1996.